

**THE UNIVERSITY OF WESTERN ONTARIO
DEPARTMENT OF CIVIL AND
ENVIRONMENTAL ENGINEERING**

Water Resources Research Report

**A generic framework to quantify
changes in floodplain regimes by
incorporating climate change
impacts over large regions**

**By:
Mohit P. Mohanty
and
Slobodan P. Simonovic**

**Report No: 112
Date: June 2021**



ISBN: (print) 978-0-7714-3157-9 ; (online) 978-0-7714-3158-6

**A generic framework to quantify changes in
floodplain regimes by incorporating climate change
impacts over large regions**



by

Mohit P. Mohanty

and

Slobodan P. Simonovic

Department of Civil and Environmental Engineering

Western University, Canada

Report No. 112

June 2021

Executive summary

The contribution of climate change towards a significant rise in severity of flood impacts and damages worldwide is well reported in the literature. In order to tackle this global issue, exhaustive floodplain mapping is considered a viable approach, which can help us identify inundated areas at different degrees of flood risk. This information can further aid in proposing appropriate flood management options to prevent damages and improve the resilience of the communities living in those areas. In recent years, with the increasing availability of publicly available datasets (e.g. climate products, digital elevation model, and river channel bathymetry details), the colossal challenge associated with data availability and accessibility has been minimized to a large extent. With the recent Coupled Model Intercomparison Project Phase 6 (CMIP6), water experts and flood modellers are curious to explore the efficacy of the new and upgraded climate models in representing flood inundation dynamics and how they will be impacted in the future by climate change. At the same time, sophisticated global flood models capable of simulating flood inundation at high resolutions have been able to overcome the challenge of performing complex simulations over large regions. With these opportunities in hand, it is now much easier than before to quantify the impacts of climate change on floodplain mapping at large scales.

This book reports a generic approach to quantify changes in floodplain regimes with climate change impacts over a large region. The book highlights the latest scientific developments with respect to the availability and application of the latest climate models in floodplain mapping. The gridded surface runoff data from the latest CMIP6 General Circulation Models under different Shared Socioeconomic Pathways (SSPs) serves as hydrological input to CaMa-Flood model, an efficient and widely used global flood model. A comprehensive framework is proposed to generate high-resolution floodplain maps that contain information on both flood inundation extent and flood depth for the near-, and far-future under various SSPs. The proposed framework is implemented in Canada. The changes in floodplain regimes is addressed by considering the changes in flood inundation extent, flood depths and changes in flood frequency. Further details on deriving regional floodplain maps from the entire floodplain map is also detailed. The report provides crucial information on data sources, and flood inundation modelling techniques to any water professional and expert working in the area of floodplain mapping.

Keywords: CaMa-Flood model; CMIP6; Floodplain mapping; Floodplain regimes; Flood risk management; Shared Socioeconomic Pathways.

Table of Contents

Executive summary	ii
Table of Contents	iii
List of Figures	iv
List of Tables	v
1. Introduction	6
1.1 Impacts of climate change on floods over the globe.....	6
1.2 Impacts of climate change on floods over Canada.....	8
1.3 Challenges in floodplain mapping over large regions.....	9
1.4 Understanding climate change impacts on floodplain mapping: Past approaches and recent developments.....	10
1.5 Sixth phase of the Coupled Model Intercomparison project(CMIP).....	11
2. List of data sources	15
2.1 Runoff data from GCMs in CMIP6 project.....	15
2.2 Catchment based Macro-Scale Floodplain (CaMa-Flood) Model.....	16
2.2.1 Components of the model.....	17
2.2.2 Model structure.....	18
3. Proposed framework and methodology	23
3.1 Accessing CMIP6 runoff data.....	24
3.2 Preparation of runoff input files to CaMa-Flood model.....	25
3.3 CaMa-Flood model simulations.....	26
3.4 Processing of outputs from CaMa-Flood.....	29
3.5 Conversion of outputs to GeoTIFF format.....	30
3.6 Flood inundation modelling (including extreme value analysis).....	30
3.7 Validation of floodplain maps.....	31
3.8 Quantifying changes in floodplain regimes for the near, and far-future.....	31
3.8.1 Quantification of changes in flood inundation extents.....	32
3.8.2 Quantification of changes in flood hazards.....	32
3.8.3 Quantification of changes in the frequency of flood events.....	33
4. Sample flood model simulation and analysis	34
4.1 Downloading runoff data from CMIP6 GCMs.....	34
4.2 Reading CMIP6 runoff data.....	36
4.3 Extracting runoff data for Canada.....	38
4.4 Converting runoff from numeric to binary format.....	39
Figure 4.8: R code for converting input runoff from numeric to binary format.....	39
4.5 Flood model simulation in SHARCNET.....	39
4.6 Clipping simulated floodplain map for a regional watershed.....	44
5. Closing Remarks	47
References	48
Appendix A: Previous Reports in the Series	52

List of Figures

Figure 1.1: Degree of exposure of world population to floods.....	6
Figure 1.2: Exposure of global population living in different countries to floods.	7
Figure 1.3: Average change in population affected (a, c, e) and expected damage (b, d, f) per country at SWLs.	8
Figure 1.4: Future CO ₂ emissions scenarios featured in CMIP6, as well as historical CO ₂ emissions (in black)..	12
Figure 1.5: Future RCP CO ₂ emissions scenarios featured in CMIP5 and their CMIP6 counterparts, as well as historical CO ₂ emissions (in black).....	13
Figure 2.1: (a) Illustration of a river channel reservoir and a floodplain reservoir defined in each grid.....	20
Figure 3.1: Proposed framework for identifying changes in floodplain regimes over Canada	23
Figure 3.2: Main page of CMIP6 available at https://esgf-node.llnl.gov/projects/cmip6/	24
Figure 3.3: CMIP6 data search and download page	25
Figure 3.4: WinSCP window login window	27
Figure 3.5: PuTTY configuration window	27
Figure 3.6: R code for Connecting to SHARCNET	28
Figure 3.7: Commands to set the modules and paths in Mkinclude file.....	29
Figure 3.8: Code to submit the jobs in PuTTY and run the code on SHARCNET.....	29
Figure 4.1: CMIP6 GCMs accessible at https://esgf-node.llnl.gov/search/cmip6/	35
Figure 4.2: List of GCMs after user selection.....	35
Figure 4.3: Interface to enter OpenID for downloading data.....	36
Figure 4.4: ESGF OpenID login interface for initiating data download.....	36
Figure 4.5: Accessing and extracting CMIP6 runoff reanalysis files.....	37
Figure 4.6: Reading runoff files.....	38
Figure 4.7: R code for extracting runoff grids lying within Canada.....	39
Figure 4.8: R code for converting input runoff from numeric to binary format.....	39
Figure 4.9: Transferring input files to the CaMa-Flood package in input folder.....	39
Figure 4.10: Logging into SHARCNET for accessing Graham server.....	40
Figure 4.11: Code compilation and creating executables in SHARCNET.....	41
Figure 4.12: Final code for running CaMa-Flood model simulation in PuTTY software.....	41
Figure 4.13: R code for converting binary data to GeoTIFF format.....	42
Figure 4.14: A representative 1 in a 100-yr floodplain map opened in QGIS.....	43
Figure 4.15: Zoomed illustration of 1 in a 100-yr floodplain map opened in QGIS.....	43
Figure 4.16: Raster clipping in QGIS.....	44
Figure 4.18: Clipped floodplain map of St. John basin from the Canada-wide floodplain map.....	45

List of Tables

Table 2.1: List of GCMs from CMIP6 project considered in this study.....	15
Table 2.2: Parameters and variables in CaMa-Flood model.....	19
Table 3.1: List of directories in the CaMa-Flood package (version 3.6.2).....	26
Table 3.2: List of floodwater related outputs generated from CaMa-flood simulation.....	29
Table 3.3 Description of performance statistics for establishing a comparison between GCM simulated and benchmark floodplain maps.....	31

1. Introduction

The recent findings by Jongman et al. (2012), Hirabayashi et al. (2013, and Wing et al. (2018) have revealed an ever-increasing exposure of economic/physical assets and human population to future flood events aggravated by climate change impacts. Winsemius et al. (2016) reported that the absolute flood damages at the global scale might intensify 20 times more by the late 21st century if sufficient proactive actions are not adopted to curb them. That is why quantifying climate change influences on future flood risk is receiving urgent attention from governments, scientists, and academic communities, in support of the search for suitable adaptation strategies and mitigation options to prevent future flood damages.

1.1 Impacts of climate change on floods over the globe

A recent report by Rentschler & Salhab (2020) highlights that around 2.2 billion people, or 29% of the world population, live in locations that are estimated to experience some level of inundation during a 1 in 100-year flood event. It further states that about 1.47 billion people, or 19% of the world population, are directly exposed to inundation depths of over 0.15 meters (**Figure 1.1**). Furthermore, for over half of this exposed population, flooding could be even higher reaching life-threatening levels, especially for children and the disabled.

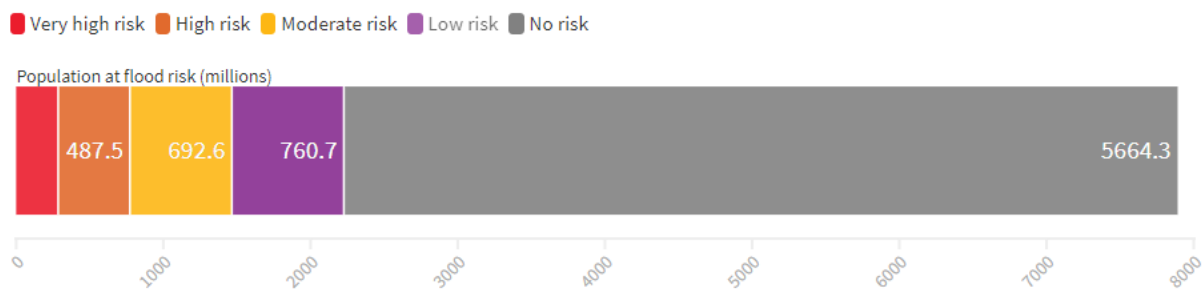


Figure 1.1: Degree of exposure of world population to floods. Here, very high risk >1.5 meter, High risk > 0.5 m, Moderate risk > 0.15 m, Low risk > 0 m (Source: Rentschler & Salhab, 2020).

It is well known that flood risk is a near-universal threat: populations are not safe in any country worldwide. Yet, the sheer number of people in harm's way is particularly large in South and East Asia. These regions are home to the majority of flood-exposed people, about 1.36 billion; with China (329 million) and India (225 million) alone accounting for over a third (**Figure 1.2**). This regional picture is explained by the fact that several large and densely populated

areas are in high-risk flood zones, such as coastal areas or low-lying river plains (for instance, along the Mekong, Brahmaputra, or Irrawaddy rivers).

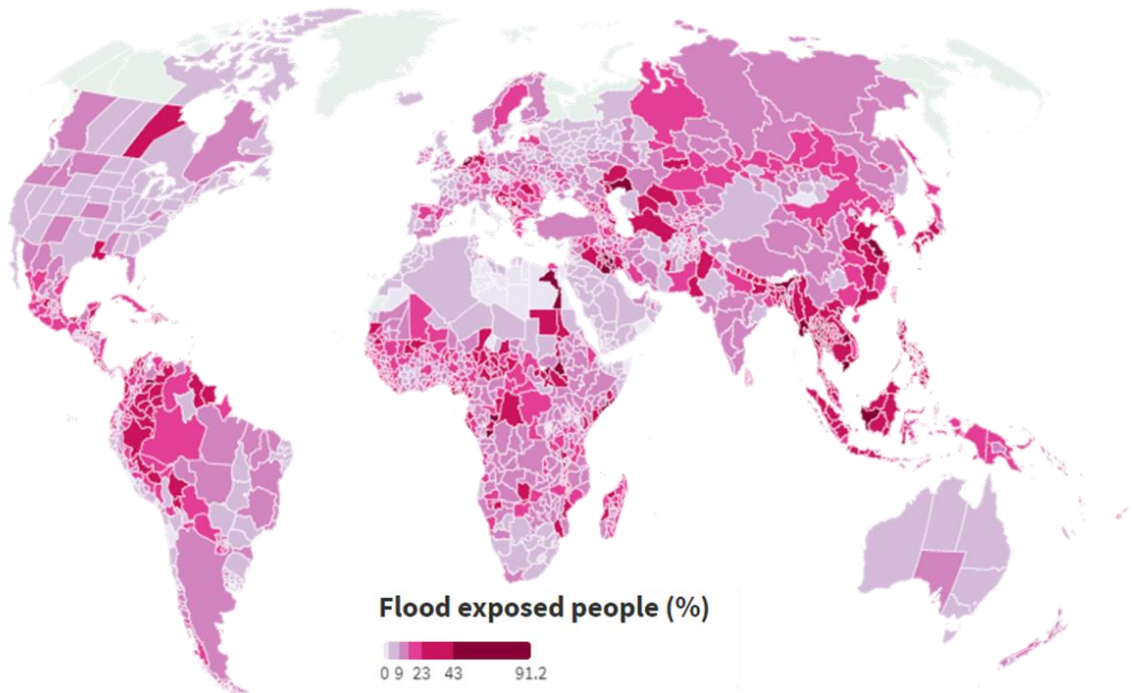


Figure 1.2: Exposure of global population living in different countries to floods (*Source:* Rentschler & Salhab, 2020).

The hydrological cycle is expected to intensify with global warming, which will likely increase the intensity of extreme precipitation events and the risk of flooding. A number of scientific findings have reported that the situation would aggravate in the near-and far-future due to climate change impacts (Milly et al., 2002; Arnell and Hughes, 2014; Dottori et al., 2018). In a significant study, Alfieri et al. (2017) determined the global changes in river flood risk at specific warming levels (SWLs) of 1.5°C, 2°C, and 4°C. The authors noticed that the changes in flood risk are unevenly distributed, with the largest increases in the Asia, U.S., and Europe (**Figure 1.3**). On the other hand, projected changes are statistically not significant in most countries in Africa and Oceania for all considered warming levels. Relative changes in population affected (damage) at 4°C warming are projected to exceed 1000% in 15 countries in Central Europe, South Asia, South America, and Japan (confidence = 90%), as compared to that in 1976–2005.

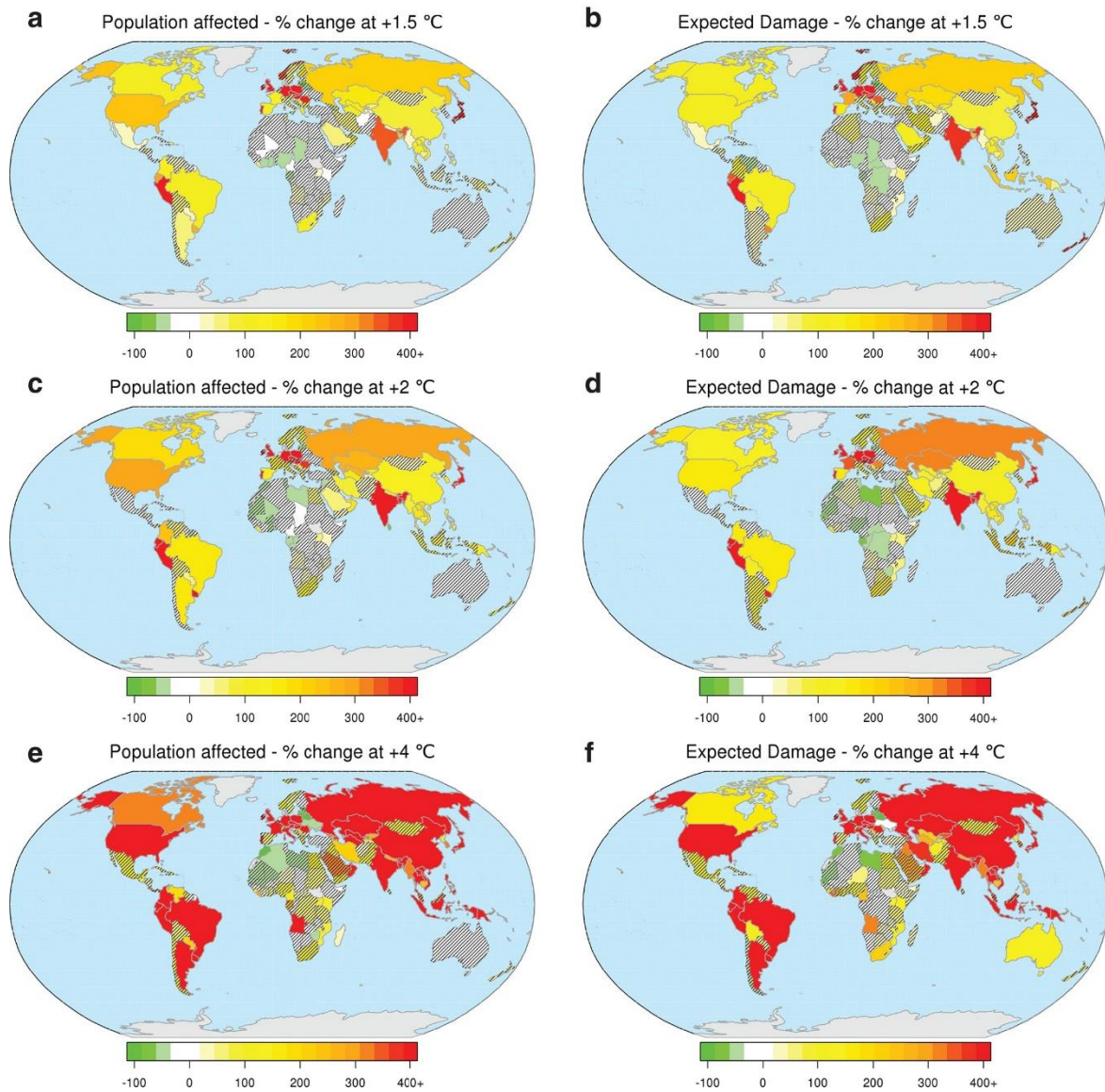


Figure 1.3: Average change in population affected (a, c, e) and expected damage (b, d, f) per country at SWLs. Hatching indicates countries where the confidence level of the average change is less than 90% (Source: Alfieri et al. 2017)

1.2 Impacts of climate change on floods over Canada

Among all-natural disasters in Canada, flood events occur quite frequently and are often referred to as the ‘*costliest natural disaster*’ (Burn & Whitfield, 2016; Oubennaceur et al., 2019). In fact, the largest portion of annual disaster recovery costs and property insurance claims is allocated towards flood damages (Henstra & Thistlethwaite, 2017). Hence, mitigating flood risks, simultaneously increasing the resilience of the affected communities, is a key concern for the federal government (Mohanty & Simonovic, 2021). Public Safety Canada (2019) indicates that the number of flood events have increased between 1970 and 2015;

Hence, mapping and mitigating flood risks has become a key challenge to ensure resilience of the affected communities.

In a motive to address this situation, the Public Safety Canada has released a set of Federal Flood Mapping Guidelines Series. The series of documents are accessible at <https://www.publicsafety.gc.ca/cnt/mrgnc-mngmnt/dsstr-prvntn-mtgtn/ndmp/fldpln-mppng-en.aspx>. An important component of these guidelines is the consideration of climate change assessments within flood risk management. Canada's National climate change assessment highlights that the surface air temperature and rainfall have increased between 1950 - 2019, particularly during the spring and fall (Bush et al., 2014). In a comprehensive analysis, Gaur et al. (2018) considered 21 GCMs from the CMIP5 project to understand the variations of flood hazards over Canada during future periods. The authors reported that the frequency of historical 1 in 100-yr flood events may fall within the range of 1 in 10 to 1 in 60-years over South-western Ontario and northern-most parts of Canada in the future. Curry et al. (2019) considered downscaled precipitation and temperature from an ensemble of 21 CMIP5 GCMs into the VIC model to derive streamflow over the Fraser River Basin, British Columbia. The authors indicate the possible occurrence of peak annual floods of record frequency by the end of this century. Several other studies carried out at regional levels have consistently shown a substantial reduction in frequency and consequent rise in the magnitude of extreme flood events over different parts of Canada (Samiran & Simonovic, 2012, Clavet-Gaumont et al., 2017).

1.3 Challenges in floodplain mapping over large regions

Floodplain mapping refers to the scientific delineation of flood extents and elevations on a base map. Additional details may be displayed on the map, including: flow velocities, depth, other risk parameters, and vulnerabilities. While several studies have performed flood mapping at local and regional scales, there was always a growing interest within the scientific community to perform at a larger scale i.e. country and global level. However, there were twin hurdles in accomplishing this goal: (i) Huge computational power to perform inundation modeling and, (ii) availability of global data sets to serve as model inputs.

The last few years have seen an explosion of global flood models to account for the difficulty linked with big-data handling and complex numerical simulations (Hoch and Trigg, 2018). These models are tailor-made to present the hydrodynamics of flow by solving hydraulics and physics-based equations. The flood hazard and risk maps are quantified from inundation outputs, which provide crucial information on the location, severity and degree of damage

(Winsemius et al., 2016; Alfieri et al., 2017). Some widely used global flood models and their sources are Catchment-Based Macro-scale (CaMa-Flood) model, Centro Internazionale in Monitoraggio Ambientale and United Nations Environment Program (CIMA-UNEP) model, European Centre for Medium-Range Weather Forecasts (ECMWF) model, Global Flood Risk (GLOFRIS) model, Joint Research Centre (JRC) model, SSBN model (now known as Fathom Global Ltd), LISFLOOD-FP. These models are now increasingly used for national flood hazard mapping and flood forecasting in many countries. In general, these models are built on two modules: (i) a method to estimate river flow for a given probability; and (ii) simulate water flow in the river channels and adjoining flood plains (Trigg et al., 2016).

1.4 Understanding climate change impacts on floodplain mapping: Past approaches and recent developments

In the quest for propelling climate-related research, the World Climate Research Programme (WCRP) initiated the Coupled Model Intercomparison Project (CMIP) in 1995 (Meehl et al., 2014). With the utilization of advanced climate models, scientists and researchers have gained deeper insights into understanding the processes and mechanisms that influence the hydro-climatological phenomenon due to climate variability. With their continuous evolution, the climate models or more commonly called General Circulation Models (GCMs), have been put to use extensively by the hydrological research community for gaining deeper knowledge on the climate change impacts on flood risk dynamics during historical, present, and future periods (Gao et al., 2019).

The CMIP has developed in phases, starting with CMIP 1 and 2 (Meehl, 1995; Meehl et al., 2000), CMIP3 (Meehl et al., 2007), CMIP5 (Taylor et al., 2012; Knutti et al., 2013), and most recently CMIP6 (Eyring et al., 2016). For the first time, the CMIP3 working group introduced the concept of ‘emission scenarios’ to depict future climate conditions based on the anticipated demographics, environmental characteristics, and socioeconomic growth (Farsani et al., 2019). Such scenarios are of particular interest to the decision-makers and policy-makers, as they provide crucial lessons for designing appropriate mitigation and adaptation strategies. With the success of CMIP3 and feedback from scientists from various backgrounds, the climate modelers in 2008 added several new dimensions to develop the CMIP5 group of GCMs (Taylor et al., 2011). The IPCC Fifth Assessment Report is based on the observations derived from the extended set of experimental simulations in the CMIP5 project (Emori et al., 2016; Touzé-Peiffer et al., 2020). CMIP5 proposed four new scenarios, also known as Representative

Concentration Pathways or RCPs, which vary from the previous scenarios in CMIP3 (IPCC, 2007). Since then, several studies have considered CMIP5 models in determining the influence of climate changes to flood risk at various spatial scales (Bajracharya et al., 2018; Lim et al., 2018; Gaur et al., 2018, 2019; Gusain et al., 2020).

In recent times, the most updated coordinated set of climate experiments have led to building the framework for phase 6 of CMIP (Eyring et al., 2016). An improved set of experiments have been considered in developing the CMIP6 GCMs. They include- (i) understanding climate extremes in the past and future, (ii) better quantification of the impact of cloud cover towards the sensitivity of climate and general atmospheric circulation (Webb et al., 2017), (iii) enhanced understanding and prediction of regional sea-level changes (Ferrero et al., 2021), (iv) determining the impacts of a warming climate on the cryosphere, (v) quantifying the factors that govern overland water availability (Trenberth and Asrar, 2014), (vi) understanding the contribution of biogeochemical cycles in controlling GHGs and subsequent climate changes (Lawrence et al., 2016), and (vii) refining near-term climate predictions (Kushnir et al., 2019).

1.5 Sixth phase of the Coupled Model Intercomparison project(CMIP)

CMIP6 represents a substantial expansion over CMIP5, in terms of the number of modelling groups participating, the number of future scenarios examined and the number of different experiments conducted. The goal of CMIP is to generate a set of standard simulations that each model will run. This allows results to be directly comparable across different models to see where models agree and disagree on future changes. One of the main sets of simulations run by models are future climate scenarios, where models are given a common set of future concentrations of greenhouse gases, aerosols and other climate forcings to project what might happen in the future.

In the lead up to the IPCC AR6, the energy modelling community has developed a new set of emissions scenarios driven by different socioeconomic assumptions. These are the “Shared Socioeconomic Pathways” (SSPs). A number of these SSP scenarios have been selected to drive climate models for CMIP6. Specifically, a set of scenarios were chosen to provide a range of distinct end-of-century climate change outcomes. Earlier, the IPCC AR5 featured four Representative Concentration Pathways (RCPs) that examined different possible future greenhouse gas emissions. These scenario- RCP2.6, RCP4.5, RCP6.0, and RCP8.5 – have new versions in CMIP6. These updated scenarios are called SSP1-2.6, SSP2-4.5, SSP4-6.0, and

SSP5-8.5, each of which result in similar 2100 radiative forcing levels as their predecessor in AR5. A number of new scenarios are also being used for CMIP6 in order to give a wider selection of futures for scientists to simulate. **Figure 1.4** shows the annual CO₂ emissions assumed under each scenario out to 2100. The new scenarios include SSP1-1.9 (purple line), SSP4-3.4 (blue solid), SSP5-3.4OS (blue dashed) and SSP3-7.0 (orange).

CO₂ emissions in CMIP6 scenarios

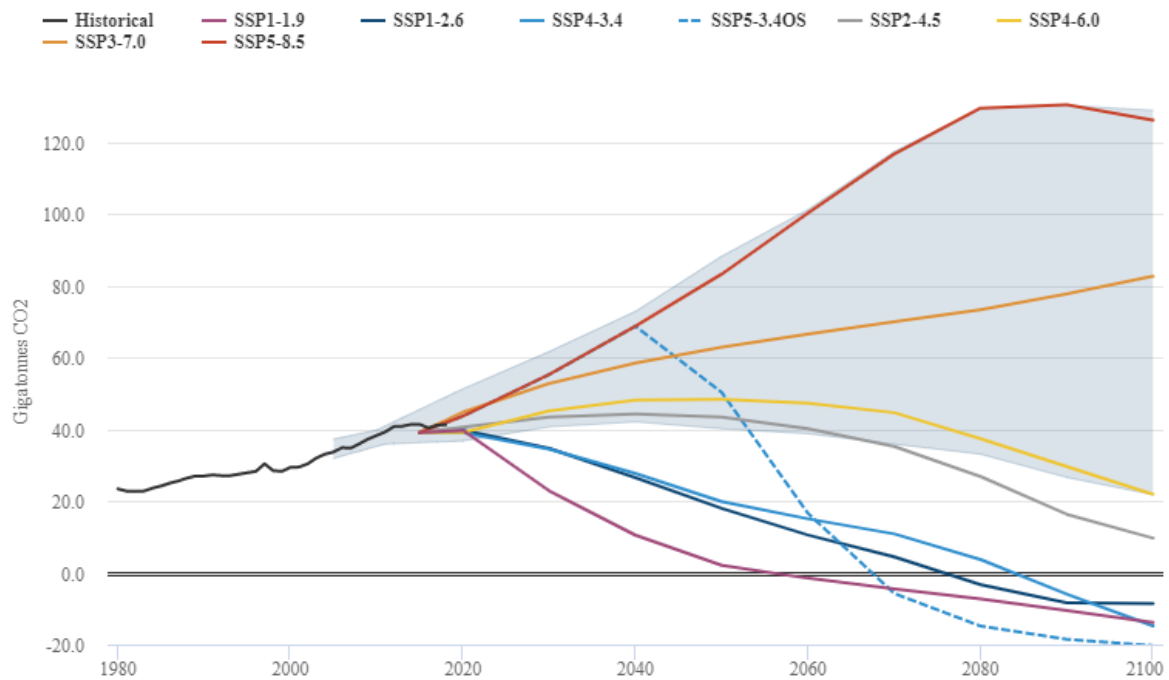


Figure 1.4: Future CO₂ emissions scenarios featured in CMIP6, as well as historical CO₂ emissions (in black). The shaded area represents the range of no-policy baseline scenarios.

One major improvement to CMIP6 scenarios is a better exploration of possible baseline “no climate policy” outcomes. The prior generation of climate models featured in CMIP5 only included one very high baseline scenario (RCP8.5) and one relatively little-mitigation scenario consistent with baseline outcomes (RCP6.0). Much of the subsequent literature relied on RCP8.5 as the only no-policy baseline, often referring to it as “business as usual” despite it being somewhat of a worst-case among possible no-policy outcomes. CMIP6 has added a new scenario SSP3-7.0, which lies right in the middle of the range of baseline outcomes produced by energy system models (**Figure 1.5**). Now modellers can examine worst case (SSP5-8.5), middle of the road (SSP3-7.0) and more optimistic (SSP4-6.0) outcomes when modelling how the world might warm in a world that fails to enact any climate policies.

SSP4-3.4 is another new scenario that tries to explore the space between scenarios that generally limit warming to below 2C (RCP2.6 / SSP1-2.6) and around 3C (RCP4.5 / SSP2-4.5) by 2100. It will help scientists better assess the impacts of warming if societies rapidly reduce emissions, but fail to mitigate fast enough to limit warming to below 2C. SSP5-3.4OS is an overshoot scenario (OS) where emissions follow a worst-case SSP5-8.5 pathway until 2040, after which they decline extremely rapidly with a lot of late-century use of negative emissions. Finally, SSP1-1.9 is a scenario intended to limit warming to below 1.5C by 2100 above pre-industrial levels. It was added in the aftermath of the Paris Agreement when countries agreed to pursue efforts to limit the temperature increase to 1.5C. The energy models and simple climate models developed to limit warming to 1.5C played a big role in the special report on 1.5C that the IPCC published in 2018. These new CMIP6 scenarios will now allow full climate models to explore climate changes and impacts at around 1.5C warming. CMIP6 features new scenarios that result in 2100 forcing similar to the CMIP5 RCP scenarios. However, even though their end-of-century forcing is the same, the emissions pathways and mix of CO₂ and non-CO₂ emissions are different. The figure below compares the CO₂ emissions in the old RCP scenarios (dashed lines) and their new SSP counterparts (solid lines).

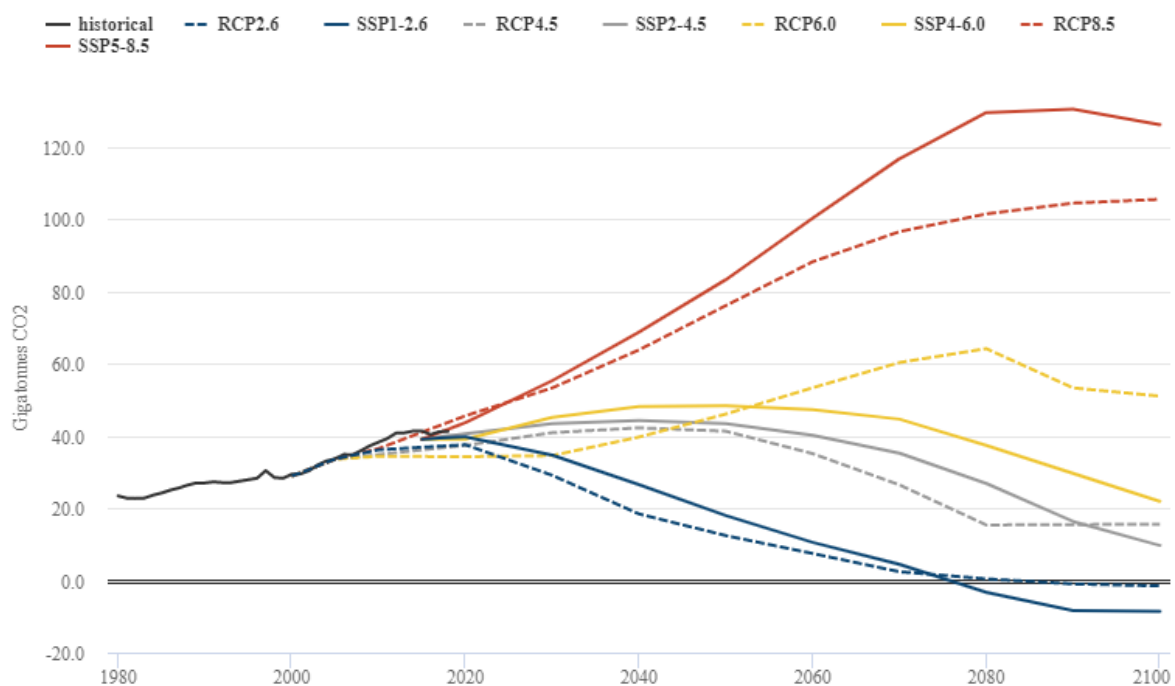


Figure 1.5: Future RCP CO₂ emissions scenarios featured in CMIP5 and their CMIP6 counterparts, as well as historical CO₂ emissions (in black).

The scientific community duly acknowledges the worth of enumerating climate change impacts on future flooding patterns. Many studies have reported on the amplification of intensity and

frequency of floods at a regional scale, leaving behind little knowledge at a national scale. At the same, a holistic understanding of future flooding patterns in terms of changes in floodplain regimes that include a combined knowledge on future flood inundation extents, flood hazards, and flooding frequency has not been addressed in any single study so far. With the increasing availability of Global Flood inundation models, it has now become easier than before to simulate flooding at large scales spanning beyond regional dimensions. Currently, there is growing interest among the scientific community in utilizing these sophisticated inundation models along with climate datasets to understand and quantify the future changes in flood plain regimes at larger scales. Moreover, the credibility of the latest GCMs from the CMIP6 project in capturing changes in flood plain regimes at large scales has not been explored so far. With several scientific developments embedded in these models, it is expected that they will be able to account for the flood dynamics more precisely than the previous counterparts.

With all these relevant studies focussed on considering impacts of climate change on floodplain mapping, it is obvious that it is now much easier than before to perform large scale floodplain mapping. With the emergence of sophisticated flood models and publicly available datasets the process has become simpler.

This technical report provides a detailed description considering climate change impacts on floodplain mapping over Canada by runoff forcing from the latest CMIP6 models. Chapter 2 discusses the various sources of data, including a description of the flood model. Chapter 3 discusses a generic methodology that has been adopted to perform flood inundation simulation over Canada starting from downloading CMIP6 runoff data, preparation of runoff inputs for CaMa-Flood; use of high computing network SHARCNET (Shared Hierarchical Academic Network) for simulation by CaMa-Flood, and post-processing of results for further analysis. Chapter 5 provides a sample simulation, which can be followed to derive floodplain map while incorporating climate change impacts.

2. List of data sources

2.1 Runoff data from GCMs in CMIP6 project

The gridded runoff data are collected from GCMs in the CMIP6 project. Considering three time scales of historical: 1980 to 2019, near-future: 2020 to 2060, and far-future: 2061 to 2100, a total of 17 GCMs were selected. The complete list of GCMs and their corresponding institutions is provided in **Table 2.1**.

Table 2.1: List of GCMs from CMIP6 project considered in this study

Sl. No.	GCM	Institution	Reference
1	MIROC6	JAMSTEC, AORI, NIES, R-CCS, Japan	Tatebe & Watanabe (2018)
2	BCC-CSM2-MR	Beijing Climate Center, China	Wu et al. (2018)
3	CanESM5	Canadian Centre for Climate Modelling and Analysis, Canada	Swart et al. (2019)
4	MRI-ESM2-0	Meteorological Research Institute, Japan	Yukimoto et al. (2019)
5	NIMS-KMA.KACE-1-0-G	National Institute of Meteorological Sciences (NIMS) and Korea Meteorological Administration (KMA)	Young et al. (2016)
6	MPI-ESM1-2-LR	Max Planck Institute for Meteorology, Germany	Wieners et al. (2019)
7	INM-CM5-0	Institute of Numerical Mathematics, Russian Academy of Sciences, Russia	Volodin et al. (2019)
8	INM-CM4-8	Institute of Numerical Mathematics, Russian Academy of Sciences, Russia	Volodin et al. (2019)
9	MPI-ESM1-2-HR	Max Planck Institute for Meteorology, Germany	Jungclaus et al (2019)
10	CMCC.CMCC-CM2-SR5	Euro-Mediterranean Center on Climate Change, Italy	Lovato et al. (2020)
11	CCCR-IITM.IITM-ESM	Indian Institute of Tropical Meteorology, India	Raghavan et al. (2019)
12	IPSL.IPSL-CM6A-LR	Institute Pierre Simon Laplace, France	Boucher et al. (2018)
13	NorESM2-MM	Norwegian Climate Centre, Norway	Bentsen et al. (2019)

Sl. No.	GCM	Institution	Reference
14	NorESM2-LM	Norwegian Climate Centre, Norway	Seland et al. (2019)
15	EC-Earth- Consortium.EC- Earth3	EC-Earth Consortium, Europe	EC-Earth (2019)
16	CSIRO- ARCCSS.ACCESS- CM2	Commonwealth Scientific and Industrial Research Organisation (CSIRO) and ARCCSS (Australian Research Council Centre of Excellence for Climate System Science)	Dix et al. (2019)
17	GFDL-CM4	NOAA Geophysical Fluid Dynamics Laboratory, USA	Guo et al. (2018)

2.2 Catchment based Macro-Scale Floodplain (CaMA-Flood) Model

The CaMa-Flood model is an efficient distributed global river routing model designed to simulate the hydrodynamics over large regions (Yamazaki et al., 2011; 2013). The global river networks are discretized into hydrological units called ‘unit-catchments’ for achieving efficient flow computation at a large scale. The water level and flooded area are diagnosed from the water storage at each unit-catchment using the sub-grid topographic parameters of the river channel and floodplains. By adopting a grid-vector hybrid river network map, which corresponds one irregular-shaped unit-catchment to one grid-box, both realistic parameterization of sub-grid topography and easy analysis of simulation results are achieved. The river discharge and flow velocity are calculated with the local inertial equation (Bates et al., 2010), along the river network map, which prescribes the upstream-downstream relationship of unit-catchments. The time evolution of the water storage, the only one prognostic variable, is solved by the water balance equation which considers inflow from the upstream cells, outflow to the downstream cell and input from runoff forcing at each unit-catchment.

The major advantage of the CaMa-Flood is the explicit representation of flood stage (water level and flooded area) in addition to river discharge. In addition to traditional model validation with gauged river discharge, it is possible to compare model simulations and satellite observations of inundation directly. The other significant advantage of the CaMa-Flood model is its high

computational efficiency of the global river simulations. The complexity of the floodplain inundation processes is reasonably approximated to a diagnostic scheme at the scale of a unit-catchment by introducing the sub-grid topographic parameters. The cost of the prognostic computation of river discharge and water storage is optimized by implementing the local inertial equation (Bates et al., 2010) and the adaptive time step scheme (Hunter et al., 2005). The high computational efficiency of the CaMa-Flood model is beneficial for computationally demanding experiments such as ensemble/long-term experiments (Pappenberger et al., 2012; Hirabayashi et al., 2013) and dynamic coupling between river routine and other hydrological schemes (Cohen et al., 2013).

The most recent model package (version 3.6.2) of CaMa-Flood is available by request at <http://hydro.iis.u-tokyo.ac.jp/~yamadai/cama-flood/>. In the current version, the global river network maps are updated by seamless connection of HydroSHEDS (below 60° N) and Global Drainage Basin Database (GDBD) (above 60° N). A new satellite-based river width from Global Width Database for Large Rivers (GWD-LR) and code for floodplain depth downscaling are also added. The flow direction is modified to keep a consistency with GWD-LR. The grid-vector-hybrid river network map (the river network maps in previous versions) is updated in order to optimize the computational efficiency of simulations using the local inertial equation. The simulation speed with the new grid-vector-hybrid map is about 150% faster than the simulation using the previous versions. The various components within the CaMa-Flood model are described in the following sections.

2.2.1 Components of the model

Flow Direction Map

The Flow direction map is represented by Flexible Location of Waterways (FLOW) method (Yamazaki et al, 2009), an upscaling algorithm which converts a high-resolution flow direction map into a coarse-resolution river network map. It also derives sub-grid-scale topographic parameters of the derived river network map, such as channel length, channel altitude, unit-catchment area, and floodplain elevation profile.

Global River Width (GWD-LR)

The Global Width Database for Large Rivers (GWD-LR) is developed by applying the algorithm to the SRTM Water Body Database and the HydroSHEDS flow direction map (Yamazaki et al., 2014). Both bank-to-bank river width and effective river width excluding islands are calculated for river channels between 60° S and 60° N. The effective river width of the GWD-LR is slightly narrower compared to the existing databases, but the relative difference is within 20% for most river channels. As the river width of the GWD-LR is calculated along the river channels of the HydroSHEDS flow direction map, it is relatively straightforward to apply the GWD-LR to global- and continental-scale river modelling as well.

Global Water Map

Global 3 arc-second Water Body Map (G3WBM) is developed using an automated algorithm to process multi-temporal Landsat images from the Global Land Survey (GLS) database. Yamazaki et al. (2015) used 33,890 scenes from 4 GLS epochs in order to delineate a seamless water body map without cloud and ice/snow gaps. Permanent water bodies were distinguished from temporary water-covered areas by calculating the frequency of water body existence from overlapping, multi-temporal, Landsat scenes. By analyzing the frequency of water body existence at 3 arc-second resolutions, the G3WBM separates river channels and floodplains more clearly than previous studies.

OSM Water Layer

OSM Water Layer is a global surface water data, generated by extracting surface water features from Open Street Map (Yamazaki et al., 2019). Both filtered OSM data (PBF format) and rasterized map (GeoTiff format) are available for usage. For generation of rasterized map, surface waters are classified into four categories, namely large Lake and River, Major River, Canal, and Minor Stream. The OSM water layer rasterized map is referenced to WGS 84. The data is available at 5 degree × 5 degree tiles (6000 pixel × 6000 pixel).

2.2.2 Model structure

The fine-resolution flow direction map from the Global Drainage Basin Database (GDBD) (Masutomi et al., 2009) is available within the model. GDBD describes the downstream direction

of each pixel at 1 km resolution in raster format. Each GDBD pixel is assumed to have only one downstream direction toward one of the eight neighboring pixels. The MERIT DEM (Yamazaki et al., 2019) is employed as an input DEM for the FLOW method. The MERIT DEM is one of the most accurate DEMs covering almost the entire globe and has a comparable spatial resolution to GDBD. Because of the difference in geometric projection between GDBD and MERIT DEM, MERIT DEM was spatially interpolated to create a surface elevation map with the same grid coordinate as GDBD. To remove the inland sinks, which interfered with flow going downstream in the surface elevation map, the elevation profile along river channels of GDBD was also smoothed.

Unit catchment and sub-grid topography

The parameters and variables used in CaMa-Flood are listed in **Table 2.2**. Each grid point over the domain has a river channel reservoir and a floodplain reservoir, as illustrated in **Figure 2.1**. The floodplain reservoir (**Figure 2.1a**) consists of the unit catchment of the river channel (**Figure 2.1b**) for each grid point, so that some areas that might never be flooded are also included in the floodplain reservoir. River channel and floodplain are treated as continuous reservoirs in that water spilling from the river channel is stored in the floodplain. This idea of assuming polygonal storages for river channels and floodplains is adapted in order to represent the realistic relationship between water storage and stage.

Table 2.2: Parameters and variables in CaMa-Flood model

Symbol	Name	Unit
Parameters		
L	channel length	m
W	channel width	m
B	bank height	m
Z	surface altitude	m
X	distance to downstream cell	m
A_c	unit catchment area	m^2
n	Manning's roughness coefficient	$m^{-1/3}s$
Variables		
S	total water storage, $S_r + S_f$	m^3
S_r	river channel water storage	m^3
S_f	floodplain water storage	m^3
D_r	river water depth	m

Symbol	Name	Unit
D_f	floodplain water depth	m
H	effective river depth	m
A_f	flooded area	m^2
R	runoff from land surface model	m/s
Q	discharge	m^3/s
R_{up}	maximum 30 day upstream runoff	m^3/s
v	river flow velocity	m/s
i_o	riverbed slope	
i_{sfc}	water surface slope	
i_f	friction slope	

A river channel reservoir has three parameters: channel length, L , channel width, W , and bank height, B . On the other hand, a floodplain reservoir has a parameter for unit catchment area, A_c , and a floodplain elevation profile, $D_f = D(A_f)$, which describes floodplain water depth, D_f , as a function of flooded area, A_f . For simplification, D_f is given as an increasing function of A_f (**Figure 2.1c**), so that no local depression is assumed in the floodplain elevation profile. This simplification is based on the assumption that inundation always occurs from lower to higher places within a unit catchment. Note that all topographic depressions, including permanent lakes and wetlands, are treated as “floodplain storages” within the framework of CaMa-Flood model.

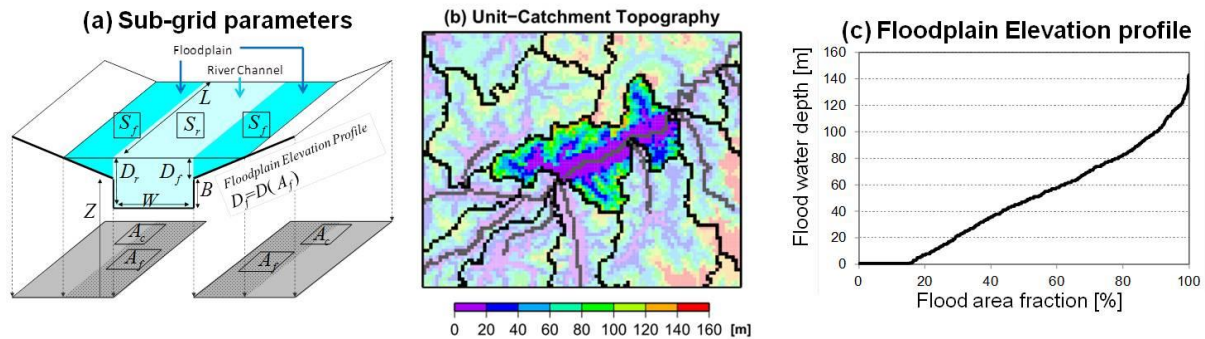


Figure 2.1: (a) Illustration of a river channel reservoir and a floodplain reservoir defined in each grid

River channel water storage, S_r , floodplain water storage, S_f , river channel water depth, D_r , floodplain water depth, D_f , and flooded area, A_f , are diagnosed from the total water storage of a grid point, S , by solving simultaneous equations (2.1 to 2.5) or (2.6 to 2.10) below. One of the simultaneous equations (2.1 to 2.5) or (2.6 to 2.10) is chosen by comparing the total water storage,

S , against the flood initiation storage, $S_{ini} = BWL$, where B is bank height, W is channel width, and L is channel length.

For cases in which total water storage, S , is less or equal to the flood initiation storage, S_{ini} .

$$S_r = S \quad (2.1)$$

$$D_r = \frac{S_r}{WL} \quad (2.2)$$

$$S_f = 0 \quad (2.3)$$

$$D_f = 0 \quad (2.4)$$

$$A_f = 0 \quad (2.5)$$

For cases in which total water storage, S , is greater than the flood initiation storage,

$$S_r = S - S_f \quad (2.6)$$

$$D_r = \frac{S_r}{WL} \quad (2.7)$$

$$S_f = \int_0^{A_f} (D_f - D(A)) dA \quad (2.8)$$

$$D_f = D_r - B \quad (2.9)$$

$$A_f = D^{-1}(D_f) \quad (2.10)$$

The equation $D_f = D_r - B$ in (2.9) means that the water surface elevations of the river channel and the floodplain are the same. This equation is based on the assumption that water mass is instantaneously exchanged between the channel and the floodplain to balance the water surface elevations of the two reservoirs. The function $D^{-1}(D_f)$, which is the inverse function of $D(A_f)$, describes flooded area, A_f , as a function of floodplain water depth, D_f (Figure 2, c). The simultaneous equations (2.6 to 2.10) are solvable because the elevation profile function, $D_f = D(A_f)$, was assumed to be an increasing function.

River network map & discharge calculation

The water exchange between the unit catchments occurs along the river network map. The river discharge is calculated with the local inertial equation (Bates et al., 2010). The local inertial equation is derived by neglecting the second term (advection) of the St. Venant's momentum expression as mentioned in equation 2.11.

$$\frac{\partial Q}{\partial t} + \frac{\partial}{\partial x} \left[\frac{Q^2}{A} \right] + \frac{gA\partial(h+z)}{\partial x} + \frac{gn^2Q^2}{R^{4/3}A} = 0 \quad (2.11)$$

The first, second, third and fourth terms represent the local acceleration, advection, water slope, and friction slope, respectively. The explicit form of the local inertial equation (2.12) is used in the CaMa-Flood model.

$$Q^{t+\Delta} = \frac{Q^t - \Delta t g A S}{\left(1 + \frac{\Delta t g n^2 |Q^t|}{R^{4/3} A} \right)} \quad (2.12)$$

The negative river discharge, which may occur in the calculation by the local inertial equation and the diffusive wave equation, represents the backward water flow from the downstream grid cell towards the current grid cell.

Storage change and flood plain flow

The storage changes at each grid cell from the time t to $t+\Delta t$ is calculated by the mass conservation as described in equation 2.13:

$$S_i^{t+\Delta t} = S_i^t + \sum_k^{upstream} Q_k^t \Delta t - Q_i^t \Delta t + A c_i R_i^t \Delta t \quad (2.13)$$

where S_i^t and $S_i^{t+\Delta t}$ represent the water storage of grid i at the time t and $t+\Delta t$, Q_i^t represents the river discharge outflow from grid i at time t , Q_k^t represents the river discharge inflow from the upstream grid k , $A c_i$ is the unit catchment area of grid i , and R_i^t represents the input runoff to the grid i . Floodplain discharge is also calculated by the local inertial equation (2.13). The flow area A is calculated by dividing floodplain storage by channel length. The flow depth h is given by the floodplain depth.

3. Proposed framework and methodology

The proposed framework for floodplain mapping over Canada is illustrated in **Figure 3.1**. Gridded daily runoff in the form of a multi-model ensemble of 17 GCMs from the CMIP6 project is used. The 17 GCMs are selected based on their common availability during three periods (i) historical: 1980 to 2019, (ii) near-future: 2020 to 2060, and (iii) far-future: 2061 to 2100.

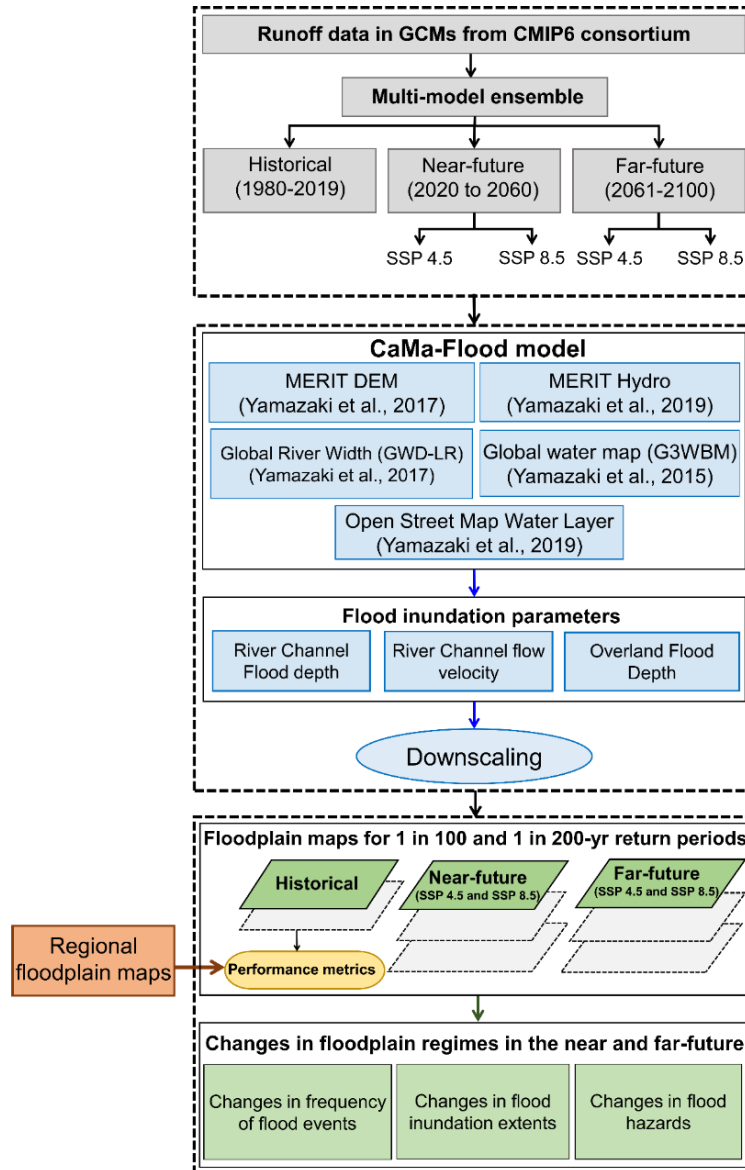


Figure 3.2: Proposed framework for identifying changes in floodplain regimes over Canada

In the present study, we consider both SSP2 4.5 (medium range of future forcing pathway) and SSP5 8.5 (high range of future forcing pathway) scenarios for the analysis. SSP2-4.5 and SSP5-8.5 scenarios update the RCP4.5 and RCP8.5 scenarios of the CMIP5 project, respectively. The GCM runoff datasets are fed to the CaMa-Flood model to produce high-resolution Canada-wide floodplain maps for 1 in 100-yr and 1 in 200-yr flood. The simulated historical floodplain maps are validated against a set of regional floodplain maps (referred to as benchmark floodplain maps from this point) over six flood-prone basins. Four widely used performance metrics are evaluated for validation. The remaining sets of floodplain maps for future scenarios are considered to understand the variations of floodplain regimes from the historical in terms of (i) changes in flood inundation extents, (ii) changes in flood hazards, and (iii) changes in the flood frequency. An exhaustive detail of the datasets and proposed methodology is outlined in the subsequent sections.

3.1 Accessing CMIP6 runoff data

The CMIP6 observations are made available by World Climate Research Programme at <https://esgf-node.llnl.gov/projects/cmip6/> as shown in **Figure 3.2**. To go to the data search and download page, the user can click on the CMIP6 search interface (red colour box highlighted).



Figure 3.1: Main page of CMIP6 available at <https://esgf-node.llnl.gov/projects/cmip6/>.

Upon clicking, a new page with a variety of options appears as shown in **Figure 3.3**. On this page, the user can select the options based on the requirements, after which a list of available datasets will be made available.



Figure 3.2: CMIP6 data search and download page

3.2 Preparation of runoff input files to CaMa-Flood model

At first, the extracted runoff datasets for Canada are interpolated to $1^\circ \times 1^\circ$ resolution on grids between 180°W to 180°E and from 90°N to 90°S as input data to the CaMa-Flood model. In the next step, the data is interpolated using Inverse Distance Squared method for filling the missing values, if any. In this method, the data at a particular grid point is considered to be inversely proportional to the square of the distance from the nearest model grid point (equation 3.1). The distance of point of interpolation is found out from four nearest reanalysis data grid points surrounding it. The interpolated value at the particular location (v_i) is calculated by finding the sum of weighted means of runoff data at all four grid points (v_j) using equation 3.2.

$$w_j = \frac{1/d_j^2}{1/d_1^2 + 1/d_2^2 + 1/d_3^2 + 1/d_4^2} \quad (3.1)$$

$$w_j = \sum_{j=1}^4 w_j \times v_j(t) \quad (3.2)$$

where d_1, d_2, d_3 and d_4 are the distances of the location of interpolation from four nearest grid points and w_j is the weight calculated for j^{th} grid point.

3.3 CaMa-Flood model simulations

The directories present in the CaMa-Flood package are tabulated in **Table 3.1**. The CaMa-Flood model simulations are performed using the SHARCNET supercomputing system (<https://www.sharcnet.ca/>). At first, one can download and install WinSCP and PuTTY.exe (as shown **Figures 3.4 and 3.5**) software packages.

Table 3.3: List of directories in the CaMa-Flood package (version 3.6.2).

Directories	Purpose
\$ (CaMa-Flood)/	Main Directory
adm/	Administration Directory, contains Mkinclude
gosh/	Shell Scripts Directory, for executing simulations
src/	Main Source Code Directory
lib/	Library Code Directory
mod/	Module Code Directory
map/	Map Directory, contains river network maps
inp/	Input Directory, contains a sample input data
out/	Output Directory, contains some programs for data processing
etc/	Various programs for analysis, visualization, etc.

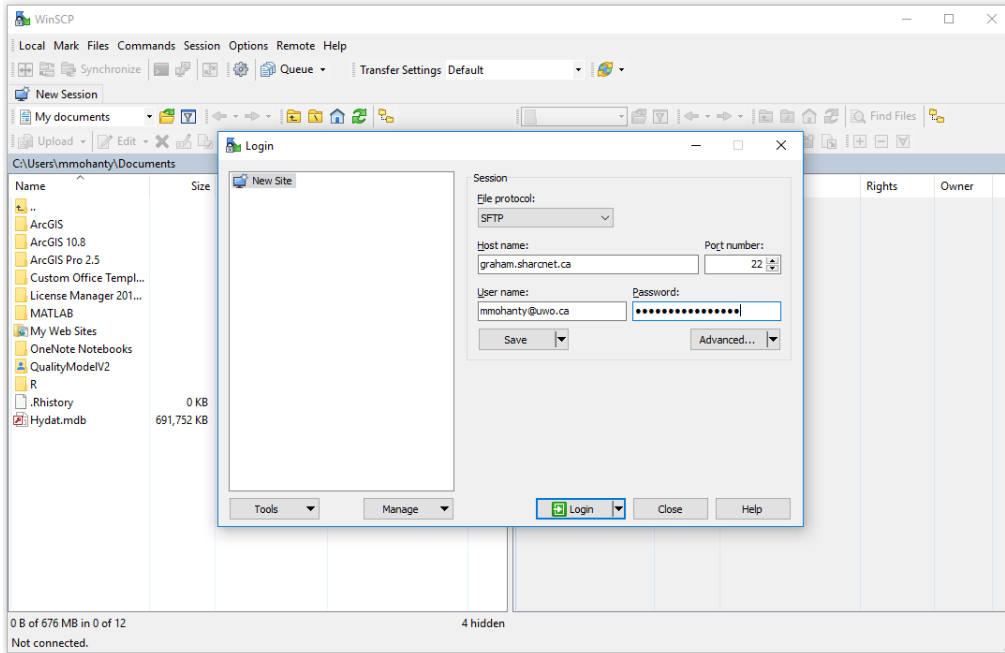


Figure 3.3: WinSCP window login window

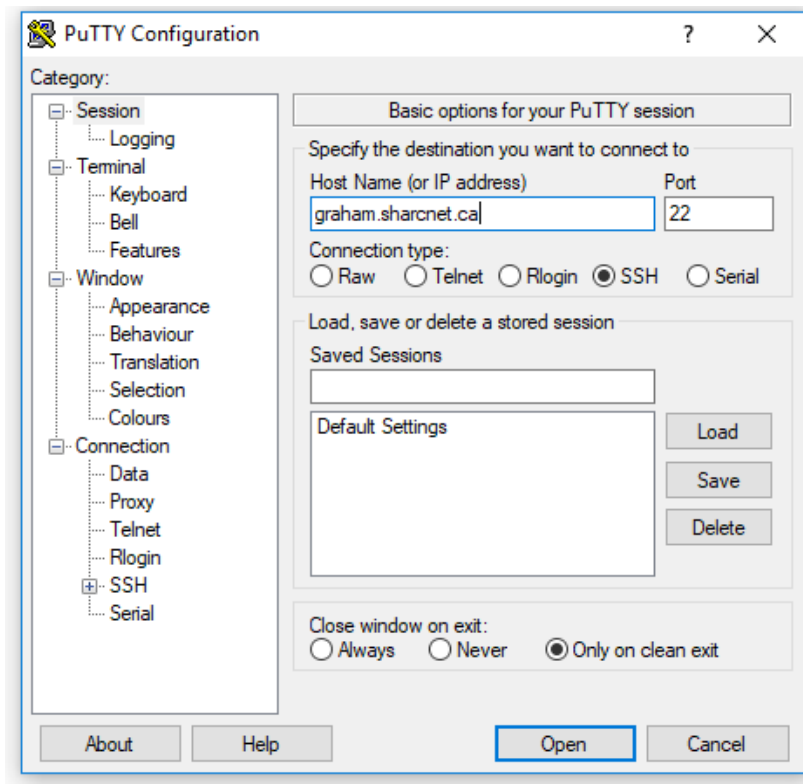


Figure 3.4: PuTTY configuration window

Once done, the modules and paths can be set by running the command as provided in **Figures 3.6 and 3.7**. By doing so, SHARCNET will be able to find “gcc” and “ifort” compiler automatically. This process should be accomplished each time the user log into SHARCNET. CaMa-flood can utilize multiple cores for model simulations. This can be set-up with the code presented in **Figure 3.8**.

```
module unload intel mkl openmpi
module load intel/15.0.6
export
LD_LIBRARY_PATH=/opt/sharcnet/testing/netcdf/4.3.2/lib:/opt/sharcnet/netcdf/4.3.2/lib:$LD_LIBRARY_PATH
```

Figure 3.5: R code for Connecting to SHARCNET

```
RM = /bin/rm -f
CP = /bin/cp
# DMPI: activate when using MPI
# DCDF: activate when using netCDF
# DEND: activate when endian conversion is needed
#DMPI=-DUseMPI
DCDF=-DUseCDF
#DEND=-DConvEnd
CFLAGS=$(DMPI) $(DCDF) $(DEND)

### gfortran ###
INC = -I/opt/sharcnet/netcdf/4.3.2/include -I/opt/sharcnet/testing/netcdf/4.3.2/include
LIB = -L/opt/sharcnet/netcdf/4.3.2/lib -L/opt/sharcnet/testing/netcdf/4.3.2/lib -lnetcdff
#-lnetcdff
CPP = gcc -E $(CFLAGS)
FC = ifort -openmp
LFLAGS =
FFLAGS = -O3 -warn all -assume byterecl -heap-arrays
# FFLAGS = -O3 -Wall -g -ffpe-trap=invalid,zero,overflow,underflow -fbounds-check -
mcmmodel=medium -fbacktrace -fdump-core
### ifort ### #INC = -I/usr/local/include
#LIB = -L/usr/local/lib -lnetcdf
#CPP = /usr/bin/gcc -E $(CFLAGS)
#FC = ifort -openmp
#FC = ifort #LFLAGS =
#FFLAGS = -O3 -warn all -assume byterecl -heap-arrays
# FFLAGS = -O3 -Wall -g -ffpe-trap=invalid,zero,overflow,underflow -fbounds-check -
mcmmodel=medium -fbacktrace -fdump-core
### ifort
```

```

### #INC = -I/usr/local/include
#LIB = -L/usr/local/lib -lnetcdf
#CPP = /usr/bin/gcc -E $(CFLAGS)
#FC = ifort -openmp
#FC = ifort
#LFLAGS =
#FFLAGS = -O3 -warn all -assume byterecl -heap-arrays
### MPI ###
#INC = -I/opt/local/include
#LIB = -L/opt/local/lib -lnetcdf
#FC = mpif90
#CPP = /usr/local/bin/gcc -E $(CFLAGS)
#LFLAGS =
#FFLAGS = -O3 -Wall

```

Figure 3.7: Commands to set the modules and paths in Mkinclude file

```

sqs sub -q threaded -n 24 -r 4h --mpp=16g -o outputfile.txt bash global_15min.sh

```

Figure 3.8: Code to submit the jobs in PuTTY and run the code on SHARCNET

3.4 Processing of outputs from CaMa-Flood

A set of 14 flood water related channel and overland outputs are generated by the CaMa-Flood model simulations as shown in **Table 3.2**. The simulated model outputs are generated in the binary format (.bin), and require conversion to numeric values for interpretation and further analysis. However, since the objective of the work presented in this report is to derive floodplain maps, we consider the Floodplain Water Depth, River Water Depth, and Flood Area for further analysis.

Table 3.4: List of floodwater related outputs generated from CaMa-flood simulation

File name	Variable	Symbol	Description	Unit	Format
rivoutYYYY.bin	rivout	Q_r	River Discharge	m ³ /s	Real
rivstoYYYY.bin	rivsto	S_r	River Water Storage	m ³	Real
rivdphYYYY.bin	rivdph	D_r	River Water Depth	m	Real
rivelYYYY.bin	rivel	V	River Flow Velocity	m/s	Real
fldoutYYYY.bin	flddph	Q_f	Floodplain Flow	m ³ /s	Real
fldstoYYYY.bin	fldsto	S_f	Floodplain Water Storage	m ³	Real

File name	Variable	Symbol	Description	Unit	Format
flddphYYYYY.bin	flddph	D_f	Floodplain Water Depth	m	Real
fldareYYYYY.bin	fldare	A_f	Flood Area	m^2	Real
fldfrcYYYYY.bin	fldfrc	F_f	Flood Fraction	m^2/m^2	Real
sfcelvYYYYY.bin	sfcelv	WSE	Water Surface Elevation	m	Real
outflwYYYYY.bin	outflw	Q_{all}	Total Discharge ($Q_r + Q_f$)	m^3/s	Real
storgeYYYYY.bin	storge	S_{all}	Total Storage ($S_r + S_f$)	m^3	Real
pthoutYYYYY.bin	pthout	Q_p	Net bifurcation flow from grid (ix, iy)	m^3/s	Real
pthflwYYYYY.pth	pthflw	--	Flow of bifurcation channel ($ipth, ilev$)	m^3/s	Real

3.5 Conversion of outputs to GeoTIFF format

After converting the requisite outputs to a numeric format, they can be converted to a GeoTIFF (Raster), for visualizing in a GIS environment. Visualizing the results in a GIS environment helps in the preparation of maps, as well as light statistical analysis without any demanding computations.

3.6 Flood inundation modelling (including extreme value analysis)

A gridded runoff matrix for 1 in 100-yr and 1 in 200-yr is generated from GCM runoff time-series data for the three time scales. In the present study, we consider Generalized Extreme Value (GEV) distribution to construct the gridded runoff values. The GEV is expressed as (Equation 3.3).

$$F(x) = \begin{cases} \exp \left[- \left(1 - \frac{k(x-\mu)}{\sigma} \right)^{1/\xi} \right] & \text{for } k \neq 0 \\ \exp \left[- \exp \left(- \frac{x-\mu}{\sigma} \right) \right] & \text{for } k = 0 \end{cases} \quad (3.3)$$

where μ is the location parameter, σ is the scale parameter, and k is the shape parameter.

In the next step, the 1 in 100-yr and 1 in 200-yr gridded runoffs along with other relevant parameters are fed to CaMa-Flood to produce Canada-wide floodplain maps. These maps contain quantitative information on river channel and overland water level (m), and overland inundation extent (km^2).

At last, a post-processing diagnostic downscaling procedure is executed on the simulated Canada-wide floodplain maps to improve the final resolution of the final maps. The downscaling procedure quantifies the simulated volume of water in the water bodies and inundated grids within the model domain. Later, it distributes the volume iteratively to the nearby hydraulically connected grids until it reaches the total volume.

3.7 Validation of floodplain maps

To confirm error-free floodplain maps with GCMs, we validated the historical floodplain maps with reference maps. The reference, or benchmark, floodplain maps have been prepared by the regional river authorities by including detailed topographical (e.g. fine-resolution topography) and hydrological (e.g. station level rainfall, observed discharge) details. These floodplain maps are available on their public platforms or were procured after contacting the river basin organizations. The floodplain maps are compared based on four performance metrics as described in **Table 3**.

Table 3.3 Description of performance statistics for establishing a comparison between GCM simulated and benchmark floodplain maps

Performance statistic	Equation*	Range and optimal value
Hit-rate	$\frac{FIE_G \cap FIE_B}{FIE_B}$	[0 to 1]; 1
False Alarm Ratio	$\frac{FIE_G / FIE_B}{(FIE_G \cap FIE_B + FIE_G / FIE_B)}$	[0 to 1], 0
Critical Success Index	$\frac{FIE_G \cap FIE_B}{FIE_G \cup FIE_B}$	[0 to 1], 1
Error Bias	$\frac{FIE_G / FIE_B}{FIE_B / FIE_G}$	[0 to ∞], a value between ‘0 and 1’ indicates underprediction, while a value between ‘1 and ∞ ’ indicates overprediction.

* FIE_G is the flood inundation extent simulated with GCMs; FIE_B is the flood inundation extent observed in the benchmark floodplain map

3.8 Quantifying changes in floodplain regimes for the near, and far-future

As highlighted before, the changes in floodplain regimes are addressed by studying the changes in

inundation extents, flood hazards, and frequency of occurrence. In this analysis, we determine the projected sign of change of runoff values while aggregating the projected changes. This approach reflects the robustness of GCMs and generates lesser uncertainty than the one that considers the median value of all GCM projections. Further details on the steps involved for quantifying differences in floodplain regimes are provided from here onwards.

3.8.1 Quantification of changes in flood inundation extents

The gridded flood inundation extent is directly obtained from the floodplain maps. The difference in inundation extents is determined at the grid level. However, for easy quantification, the difference is represented at the drainage basin by aggregating the total number of flooded grids within it. The percentage difference of flood inundation extent over a drainage basin from the historical period is calculated as per Equation 3.

$$\Delta\text{FIE} (\%) = \frac{\text{FIE}_f - \text{FIE}_h}{\text{FIE}_h} \times 100 \quad (3.4)$$

where $\Delta\text{FIE} (\%)$ is the percentage change in flood inundation extent, FIE_f is the flood inundation extent (km^2) in the 1 in 100-yr or 1 in 200-yr flood of near-future or far-future, and FIE_h is the corresponding flood inundation extent (km^2) during the historical time period.

3.8.2 Quantification of changes in flood hazards

Flood hazard is determined qualitatively by discretizing the entire range of flood depths into various classes.

Mathematical derivation of flood hazard

Let ' (d_n) ' be the flood inundation depth corresponding to any n^{th} grid ($\sim 90 \text{ m} \times 90 \text{ m}$ grid size) in the floodplain map. The flood hazard given as \mathcal{H} is based on $d_n \in \mathbf{D} \forall n \in \mathbf{N}$. Here \mathbf{D} represents the complete set of inundated grids. Hence, \mathcal{H} is an $f(\mathbf{D})$ and can be expressed as in Equation 4:

$$\psi: \mathbf{D} \rightarrow \mathcal{H} \in \mathbf{R}_+ \mid \mathcal{h} = \psi((d_1), \dots, (d_n)); \mathcal{h} \in \mathcal{H}; n \in \mathbf{N}, \text{ and } (d_1), \dots, (d_n) \in \mathbf{C} \quad (3.5)$$

Here \mathbf{R}_+ refers to the set of positive real numbers.

The inundation values are classified into five different classes, which are designed based on the impacts on economic/physical assets and population. The following mapping is implemented on \mathcal{H} (Equations 5 & 6)

$$\omega_z: \mathcal{H} \rightarrow \mathcal{H}_d; \mathcal{H}_d = \{\hbar_d \in \mathbb{N}: \hbar_d \leq 5 \quad (3.6)$$

$$\hbar_d = \begin{cases} \text{very-low, } 0 \leq \hbar \leq 0.2 \\ \text{low, } 0.2 < \hbar \leq 0.6 \\ \text{medium, } 0.6 < \hbar \leq 1.5 \\ \text{high, } 1.5 < \hbar \leq 3.5 \\ \text{very-high, } \hbar > 3.5 \end{cases} \quad (3.7)$$

Here \hbar is the value of flood hazard for the n^{th} grid, and \hbar_d is the flood hazard index for the n^{th} grid. Based on the methodology, a suite of Canada-wide flood hazard maps are prepared for the historical and future time periods. The difference in flood hazard from the historical time period is determined for each grid, as per Equation 7:

$$\Delta \mathcal{H}^i (\%) = \frac{\mathcal{H}_f^i - \mathcal{H}_h^i}{\mathcal{H}_h^i} \times 100 \quad (3.8)$$

where $\Delta \mathcal{H}^i (\%)$ is the change in flood hazard for the i^{th} grid, \mathcal{H}_f^i and \mathcal{H}_h^i are the flood hazard observed during future and historical periods for the i^{th} grid.

3.8.3 Quantification of changes in the frequency of flood events

In order to quantify the changes in the frequency of flood events, the gridded runoff for historical and future was considered. In this analysis, we focus on the changes in frequencies of the historical flood events for 1 in 100 and 1 in 200-yr during the far-future period. The annual maximum runoff time series for the historical period was modelled using GEV distribution. The flow quantiles for both 1 in 100 and 1 in 200-yr were estimated. The same procedure was carried out on annual maximum runoffs of the far-future, based on which the changes in return periods of flood events were identified.

4. Sample flood model simulation and analysis

This section provides a detailed description to consider future runoff values as inputs to the CaMa-Flood model to derive high resolution floodplain maps. A total of 17 CMIP6 GCMs were considered that are common to the three time frames as discussed before. The runoff data is available at a daily time scale. A set of R code programs are used to access the runoff files, extract and process the runoff to be used as inputs to the CaMa-Flood. The step-wise procedure includes: (i) downloading CMIP6 runoff data, (ii) reading runoff data, (ii) extracting runoff values for Canada, (iii) converting runoff from numerical to binary format, (iv) flood model simulation in SHARCNET, (v) conversion of simulated files to GeoTIFF, and (vi) Clipping simulated floodplain map for a regional watershed.

4.1 Downloading runoff data from CMIP6 GCMs

The daily CMIP6 runoff data is available at <https://esgf-node.llnl.gov/search/cmip6/> as shown in **Figure 4.1**. In this page, the user can see a variety of options to select from in the left panel. Since runoff is the desired hydrological variable in our case, we should select ‘mrros’; the abbreviation for surface runoff. The remaining options should be- CMIP6 (MIP Era), model-output (Product), r1i1p1f1 (Variant Label). In the experiment ID option, various scenarios pertaining to SSPs are available. For a sample simulation, we have selected ssp585. After selecting the appropriate options, the complete list of models and their details appears in the central panel of the page. One can select the options below each GCM to view more details about the data. To download the files, select ‘show files’ icon. This will list down the files of the selected GCM (**Figure 4.2**). There are two options to download- HTTP download and OpenDAP download. Upon clicking on HTTP download, the next page will ask for entering OpenID. The user can enter the ID if there exists (**Figure 4.3**), otherwise they can create a new account.

Home Contact Us Data Nodes Status

WARNING: Not all models include a variant 'r11p1f1', and across models, identical values of variant_label do not imply identical variants! To learn which forcing datasets were used in each variant, please check modeling group publications and documentation provided through ES-DOC.

CMIP6 project data downloads are unrestricted. Downloads should be performed with the -s option to a wget script without the need to login. When using this method for download, ensure you are not using additional options, eg. -s and -H should never be combined.

Enter Text: Display results per page [\[More Search Options \]](#)

Show All Replicas Show All Versions Search Local Node Only (Including All Replicas)

Search Constraints: CMIP6 | r11p1f1 | model-output | ssp585 | mrros

Total Number of Results: 34
-1- 2 3 4 Next >>
Please login to add search results to your Data Cart
Expert Users: you may display the search URL and return results as XML or return results as JSON

1. CMIP6.ScenarioMIP.MRI.E.SM2.0.ssp585.r11p1f1.Lmon.mrros.gn
Data Node: esgf-data2.diasjp.net
Version: 20191108
Total Number of Files (for all variables): 2
Full Dataset Services: [\[Show Metadata \]](#) [\[List Files \]](#) [\[WGET Script \]](#) [\[Show Citation \]](#) [\[PID \]](#) [\[Further Info \]](#)
2. CMIP6.ScenarioMIP.MIROC.MIROC6.ssp585.r11p1f1.Lmon.mrros.gn
Data Node: esgf-data2.diasjp.net
Version: 20190627
Total Number of Files (for all variables): 1
Full Dataset Services: [\[Show Metadata \]](#) [\[List Files \]](#) [\[WGET Script \]](#) [\[Show Citation \]](#) [\[PID \]](#) [\[Further Info \]](#)
3. CMIP6.ScenarioMIP.CAS.FGOAL.S-F3-L.ssp585.r11p1f1.Lmon.mrros.gn
Data Node: esg.lasg.ac.cn is reported as unavailable. Any existing replica data sets can be seen by selecting 'Show All Replicas'.
Version: 20190821
Total Number of Files (for all variables): 1
Full Dataset Services: [\[Show Metadata \]](#) [\[List Files \]](#) [\[WGET Script \]](#) [\[LAS \]](#) [\[Show Citation \]](#) [\[PID \]](#) [\[Further Info \]](#)
4. CMIP6.ScenarioMIP.CCma.CanE.SM5.ssp585.r11p1f1.Lmon.mrros.gn
Data Node: crd-esgf-drc.ec.gc.ca
Version: 20190429
Total Number of Files (for all variables): 3
Full Dataset Services: [\[Show Metadata \]](#) [\[List Files \]](#) [\[WGET Script \]](#) [\[LAS \]](#) [\[Show Citation \]](#) [\[PID \]](#) [\[Further Info \]](#)
5. CMIP6.ScenarioMIP.BCC.BCC-C.SM2-MR.ssp585.r11p1f1.Lmon.mrros.gn
Data Node: cmip.bcc.cma.cn
Version: 20190308
Total Number of Files (for all variables): 1
Full Dataset Services: [\[Show Metadata \]](#) [\[List Files \]](#) [\[WGET Script \]](#) [\[LAS \]](#) [\[Show Citation \]](#) [\[PID \]](#) [\[Globus Download \]](#) [\[Further Info \]](#)
6. CMIP6.ScenarioMIP.THU.CIE.SM.ssp585.r11p1f1.Lmon.mrros.gn
Data Node: cmip.dess.tsinghua.edu.cn
Version: 20200417
Total Number of Files (for all variables): 2

Figure 4.1: CMIP6 GCMs accessible at <https://esgf-node.llnl.gov/search/cmip6/>.

Experiment ID: ssp585 (34)

Sub-Experiment:

Variant Label: r11p1f1 (34)

Grid Label:

Table ID:

Frequency:

Realm:

Variable: mrros (34)

CF Standard Name:

Data Node:

1. CMIP6.ScenarioMIP.MRI.E.SM2.0.ssp585.r11p1f1.Lmon.mrros.gn
Data Node: esgf-data2.diasjp.net
Version: 20191108
Total Number of Files (for all variables): 2
Full Dataset Services: [\[Show Metadata \]](#) [\[Hide Files \]](#) [\[WGET Script \]](#) [\[Show Citation \]](#) [\[PID \]](#) [\[Further Info \]](#)

Total Number of Files: 2

1	mrros_Lmon_MRI-ESM2-0_ssp585_r11p1f1_gn_201501-210012.nc checksum: b54e18380f727a217bfc94ad15671c80c1c939e6ca8f89dd1c0b09075abc47dc size: 21229098 tracking_id: hdl:21.14100/21343dd5-8414-4b63-a8ac-bdf682c7d1c0 [More File Metadata]	Single File Access: HTTP Download OpenDAP Download
2	mrros_Lmon_MRI-ESM2-0_ssp585_r11p1f1_gn_210101-230012.nc checksum: 42b0abf01d80f8a771c878a7409e6ee003708c4b7c0b2585f52bcc7480cc7107 size: 50217489 tracking_id: hdl:21.14100/d9d46041-c1c0-4c97-b15a-8d562f903078 [More File Metadata]	Single File Access: HTTP Download OpenDAP Download

2. CMIP6.ScenarioMIP.MIROC.MIROC6.ssp585.r11p1f1.Lmon.mrros.gn
Data Node: esgf-data2.diasjp.net
Version: 20190627
Total Number of Files (for all variables): 1
Full Dataset Services: [\[Show Metadata \]](#) [\[List Files \]](#) [\[WGET Script \]](#) [\[Show Citation \]](#) [\[PID \]](#) [\[Further Info \]](#)
3. CMIP6.ScenarioMIP.CAS.FGOAL.S-F3-L.ssp585.r11p1f1.Lmon.mrros.gn
Data Node: esg.lasg.ac.cn is reported as unavailable. Any existing replica data sets can be seen by selecting 'Show All Replicas'.
Version: 20190821
Total Number of Files (for all variables): 1
Full Dataset Services: [\[Show Metadata \]](#) [\[List Files \]](#) [\[WGET Script \]](#) [\[LAS \]](#) [\[Show Citation \]](#) [\[PID \]](#) [\[Further Info \]](#)

Figure 4.2: List of GCMs after user selection

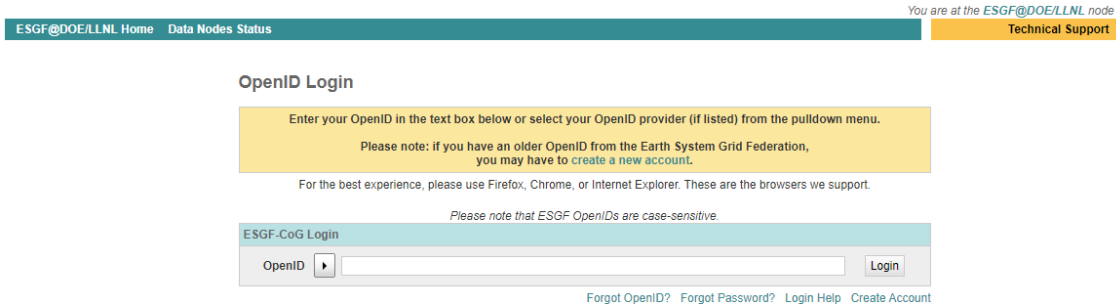


Figure 4.3: Interface to enter OpenID for downloading data

Once a new account is created, then the user can enter the relevant password to enter again, and start downloading the files (**Figure 4.4**).



Figure 4.4: ESGF OpenID login interface for initiating data download

This data is available in NetCDF format. NetCDF is a set of self-describing software libraries, machine-independent data formats that support the creation, access, and sharing of array-oriented scientific data. NetCDF files also contain dimensions, which describe the extent of the variables arrays. Files not only contain the ‘data’ but also a description of the variables, the creation history, and any other important attributes of the data set. Version 4 of the NetCDF library stores data in HDF5 format files; while earlier versions store data in a custom format.

4.2 Reading CMIP6 runoff data

The CMIP6 runoff files in NetCDF file format are accessed in R using the function provided in **Figures 4.5 and 4.6**. The runoff files are used to extract longitude, latitude information and time indices are extracted from the ‘.nc’ file, and interpolation is performed to read the ‘.nc’ runoff files. Some additional packages like *ncdf4*, *lubridate*, *ggplot2*, *reshape2* along with *ncdf4*, are used for

performing various other tasks. For example, *ncdf4* is used to access ‘.nc’ GCM files, *lubridate* is used for dates related functions, *ggplot2* and *reshape2* for plotting purposes, etc.

```
library(ncdf4)
library(lubridate)
library(ggplot2)
library(reshape2)
library(rgdal)

ncfile="C:/CMIP6_runoff/ MRI-ESM2-0/runoff_nc/runoff2020.nc"

stationlist=data.frame(Lon=c(-100,-90,-80,-120,-150,-130,-120)
Lat=c(50,60,70,85,75,65,55)
ncfiles=list.files("W:/ CMIP6_runoff/ MRI-ESM2-0/runoff_nc/",pattern="mrros.*.nc",full.names=T)
varname="mrros"
stationlist=data.frame(Lon=rep(seq(-180,179,by=1),times=180)
Lat=rep(seq(90,-89,by=-1),each=360))
write.csv(stationlist," CMIP6_runoff/ MRI-ESM2-0/runoff_nc/Results_CMIP6_MRI-ESM2-0/runoff_values.csv")
```

Figure 4.5: Accessing and extracting CMIP6 runoff reanalysis files

```
library(ncdf4)
getwd()
setwd("C:/CMIP6_runoff/ MRI-ESM2-0/runoff_nc/runoff2020.nc")
ncname="cru10min30_tmp"
ncfname=paste(ncname,".nc", sep="")
dname="tmp"
ncin=nc_open(ncfname)
print(ncin)
lon=ncvar_get(ncin,"lon")
nlon=dim(lon)
head(lon)
lat=ncvar_get(ncin,"lat",verbose=F) nlat=dim(lat)
head(lat)
print(c(nlon,nlat))

trial$dim
trial$dim$time
trial$dim$lon
trial$dim$lat
trial$dim
trial$var
trial.out=ncvar_get(nc = trial, start = 1, count = 12,varid="time")
view (trial.out)
#getting the dimensions of variable"tmp"
tmp_array=ncvar_get(nc=trial,
varid="tmp",start=c(1,1,1),count=c(720,360,1),verbose=FALSE)
tmp_array=ncvar_get(nc=trial, varid="tmp",verbose=FALSE)
dim(tmp_array)
#checking the current workspace
ls()
nc_close(ncin)
```

```

CMIP6runoff=nc_open("C:/CMIP6_runoff/ MRI-ESM2-0/runoff_nc/runoff2020.nc ")

library(lubridate)
ncvar_get(CMIP6runoff,varid="ssrun",start=c(1,1,1),count=c(349,277,1))
dim(ncvar_get(CMIP6runoff,varid="ssrun"))
coord=data.frame(lon=matrix(ncvar_get(CMIP6runoff,varid="lon"),ncol=1),lat=matrix(
ncvar_get(CMIP6runoff,varid="lat")),ncol=1)
coord=data.frame(lon=matrix(ncvar_get(CMIP6runoff,varid="lon"),ncol=1),lat=matrix(
ncvar_get(CMIP6runoff,varid="lat")),ncol=1)
head(coord)
as.Date("1800-01-01")+1691808/24
as.Date("1900-01-01")+20000
coord=data.frame
(lon=matrix(ncvar_get(CMIP6runoff,varid="lon"),ncol=1),lat=matrix(ncvar_get(CMIP6r
unoff,varid="lat"),ncol=1),ssrun=matrix(ncvar_get(CMIP6runoff,varid="ssrun"),ncol=
1))
head(coord,5)

RCP8.5_Runoff=nc_open("C:/CMIP6_runoff/MRI-ESM2-0/runoff_nc/runoff2020.nc
/Runoff_Daily_RCP8.5_2006-2100/mrros_day_MRI-ESM2-0_rcp85_r1i1p1f1_20060101-
21001231.nc")
RCP8.5_Runoff$dim$lat
RCP8.5_Runoff$dim$lon
RCP8.5_Runoff$dim$time
dim(ncvar_get(RCP8.5_Runoff,varid="lon"))
dim(ncvar_get(RCP8.5_Runoff,varid="lat"))
dim(ncvar_get(RCP8.5_Runoff,varid="time"))
tmp_array[tmp_array==fillvalue$value]=NA
length(na.omit(as.vector(tmp_array[,1])))

grid <- expand.grid(lon=lon, lat=lat)
cutpts <- c(-50,-40,-30,-20,-10,0,10,20,30,40,50)
levelplot(tmp_slice ~ lon * lat, data=grid, at=cutpts, cuts=11,
pretty=T,col.regions=(rev(brewer.pal(10,"RdBu"))))
Data=matrix(c(1,2,3,4,5,6),nrow=2)
Data
library(chron)
library(lattice)
library(RColorBrewer)
grid=expand.grid(lon=lon,lat=lat)
cutpts=c(-50,-40,-30,-20,-10,0,10,20,30,40,50)

```

Figure 4.6: Reading runoff files

4.3 Extracting runoff data for Canada

Once the CMIP6 runoff data is accessed, the next step is to extract the runoff grids lying within Canada. In order to do this, a data-frame “grids.cama.input” is prepared with coordinate extent of Canada as per the code provided in **Figure 4.7**.

```

grids.cama.input=data.frame(lon=rep(seq(-
180,179.75,by=1),times=180,lat=rep(seq(90,-89,by=-1),each=360))

```

Figure 4.7: R code for extracting runoff grids lying within Canada

4.4 Converting runoff from numeric to binary format

After extracting the runoff values, the next step is to convert the numeric data to binary format, in order to be used as input to the flood model (Figure 4.8).

```

SUB.write.daily.bin=function(runoff.day,date.day,scenario)
writeBin(object=runoff.day, endian="little", size=4, con=paste("C:/CMIP6/ MRI-ESM2-
0/CamaFlood runoff ",100YR,"/Roff_____",date.day,".one",sep=""))

```

Figure 4.8: R code for converting input runoff from numeric to binary format

4.5 Flood model simulation in SHARCNET

Once the inputs are prepared, the data input, location and outputs should be specified in the WinSCP, so that they can be accessed by the CaMa-Flood model. Desirable outputs if any, can also be fixed by making changes in this file. Modules and paths should be set in Mkinclude file before running the CaMa-Flood for runoff simulations. The Input runoff files should be transferred from the destination folder to the CaMa-Flood package through WinSCP as shown in **Figure 4.9**.

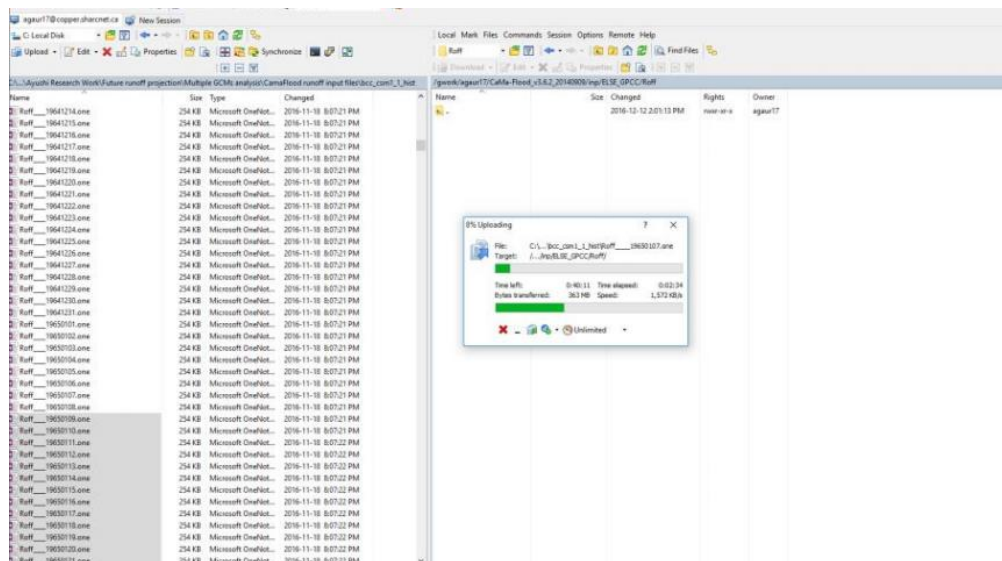


Figure 4.9: Transferring input files to the CaMa-Flood package in input folder

The following steps can be followed for performing a simulation in CaMa-Flood:

- Launch PUTTY as shown in **Figure 4.10**. Enter the login and password details corresponding to the host name. In this case, the host is Graham server of the SHARCNET. In doing so, it will open a screen, where we have to reenter the password to access the server.
- After logging in to the server, the compilation and creation of CaMa-Flood model is established as highlighted in Yellow colour in **Figure 4.11**. Next, “bash compile.sh yes” is used to start running CaMa-Flood model as shown in **Figure 4.12**. A unique job-id and status also appears on the screen that will show the progress of simulation.

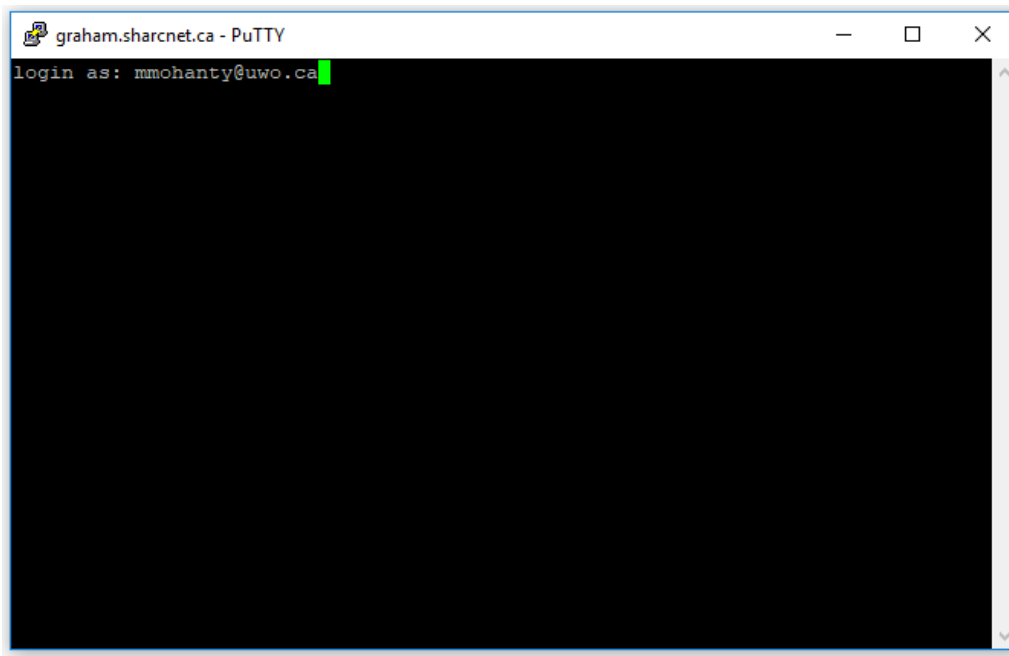


Figure 4.10: Logging into SHARCNET for accessing Graham server

```

graham.sharcnet.ca - PuTTY
ifort -openmp day2mon.o -o day2mon -L/opt/sharcnet/netcdf/4.3.2/lib
ar -rv srcs.a calc_fldstg.o calc_rivout.o calc_fldout.o calc_pthout.o calc_damout.o calc_outpre.
o calc_rivout_kine.o calc_stonxt.o calc_watbal.o create_outcdf.o create_outbin.o control_inp.o c
ontrol_phy.o control_out.o control_rest.o control_tstp.o init_inputnam.o init_map.o init_topo.o
init_cond.o init_time.o control0.o
r - calc_fldstg.o
r - calc_rivout.o
r - calc_fldout.o
r - calc_pthout.o
r - calc_damout.o
r - calc_outpre.o
r - calc_rivout_kine.o
r - calc_stonxt.o
r - calc_watbal.o
r - create_outcdf.o
r - create_outbin.o
r - control_inp.o
r - control_phy.o
r - control_out.o
r - control_rest.o
r - control_tstp.o
r - init_inputnam.o
r - init_map.o
r - init_topo.o
r - init_cond.o
r - init_time.o
r - control0.o
ifort -openmp -O3 -warn all -assume byterecl -heap-arrays MAIN_day.o srcs.a ../mod/mods.a ../l
ib/libs.a -o MAIN_day -L/opt/sharcnet/netcdf/4.3.2/lib
Compilation OK! Executable created: /work/reanalysis/CaMa-Flood_v3.6.2_20140909/gosh/./src/MAIN_d
ay

```

Figure 4.11: Code compilation and creating executables in SHARCNET

```

graham.sharcnet.ca - PuTTY
ifort -openmp -c -O3 -warn all -assume byterecl -heap-arrays -I/opt/sharcnet/netcdf/4.3.2/inclu
de day2mon.f90 -o day2mon.o
ifort -openmp day2mon.o -o day2mon -L/opt/sharcnet/netcdf/4.3.2/lib
ar -rv srcs.a calc_fldstg.o calc_rivout.o calc_fldout.o calc_pthout.o calc_damout.o calc_outpre.
o calc_rivout_kine.o calc_stonxt.o calc_watbal.o create_outcdf.o create_outbin.o control_inp.o c
ontrol_phy.o control_out.o control_rest.o control_tstp.o init_inputnam.o init_map.o init_topo.o
init_cond.o init_time.o control0.o
r - calc_fldstg.o
r - calc_rivout.o
r - calc_fldout.o
r - calc_pthout.o
r - calc_damout.o
r - calc_outpre.o
r - calc_rivout_kine.o
r - calc_stonxt.o
r - calc_watbal.o
r - create_outcdf.o
r - create_outbin.o
r - control_inp.o
r - control_phy.o
r - control_out.o
r - control_rest.o
r - control_tstp.o
r - init_inputnam.o
r - init_map.o
r - init_topo.o
r - init_cond.o
r - init_time.o
r - control0.o
ifort -openmp -O3 -warn all -assume byterecl -heap-arrays MAIN_day.o srcs.a ../mod/mods.a ../l
ib/libs.a -o MAIN_day -L/opt/sharcnet/netcdf/4.3.2/lib
Compilation OK! Executable created: /work/reanalysis/CaMa-Flood_v3.6.2_20140909/gosh/./src/MAI
ay
-bash-4.1$ sqsub -q threaded -n 24 -r 4h --mpp=16g -o output.txt bash global_15min.sh
submitted as jobid 337887
-bash-4.1$ sqjobs
  jobid  queue state ncpus nodes time command
-----
337887  threaded  R      24  cop28  17s  bash global_15min.sh
-bash-4.1$

```

Figure 4.12: Final code for running CaMa-Flood model simulation in PuTTY software

- Once the model simulations are complete, we can go back to the folder meant to store the relevant outputs. The results are in the binary format, which can be converted to numeric format and GeoTIFF as per the code in **Figure 4.13**.

```

function [temp,header]=ctltoRaster(Df,Latlim,Lonlim,xx,yy,outfile)
%file_name='C:\Runoff\MRI-ESM2-0_100YR_result\flddph.ct1';
tempS=Df(:,:,1,:);
temp=mean(tempS,4);
[m,n]=size(temp);
mValue=max(max(temp));
for i=1:m
    for j=1:n
        if abs(temp(i,j)-mValue)<0.001
            temp(i,j)=0;
        end
    end
end
end
%[x,y] = meshgrid([72:0.005:135.9950],[-179.875:0.25:179.8750]);

% surf(x,y, temp)
%
% [Plg,Plt]=meshgrid([-89.875:0.25:89.875],[-179.875:0.25:179.8750]);
%
% m_proj('hammer-aitoff','clongitude',-150);
% m_pcolor(Plg,Plt,temp);shading flat;
% hold on;
% m_coast('patch',[.6 1 .6]);
% m_grid('xaxis','middle');
%
% % add a standard colorbar.
% h=colorbar('h');
% set(get(h,'title'),'string','MRI-ESM2-0_100YR_result ');
%
% hold off

R = georasterref('RasterSize', [xx yy ], ...
    'RasterInterpretation', 'cells', ...
    'Latlim',Latlim,'Lonlim',Lonlim, ...
    'ColumnsStartFrom', 'north');
geotiffwrite(outfile,temp',R)

```

Figure 4.13: R code for converting binary data to GeoTIFF format

- The GeoTIFF file can be opened in a GIS platform directly to visualize the flood inundation depth and extent values. Since the result does not come with any geographic projection, it is necessary to define a new projection ‘D_WGS_1984’ to ensure the boundary of Canada and floodplain maps match accurately. A larger domain of reanalysis data extent is considered, hence the results within Canada can be clipped by using ‘Clip Raster’ option. A representative floodplain map for 1 in 100-yr return period opened in QGIS is illustrated in **Figure 4.14**. A zoomed picture of the same map is provided in **Figure 4.15**.

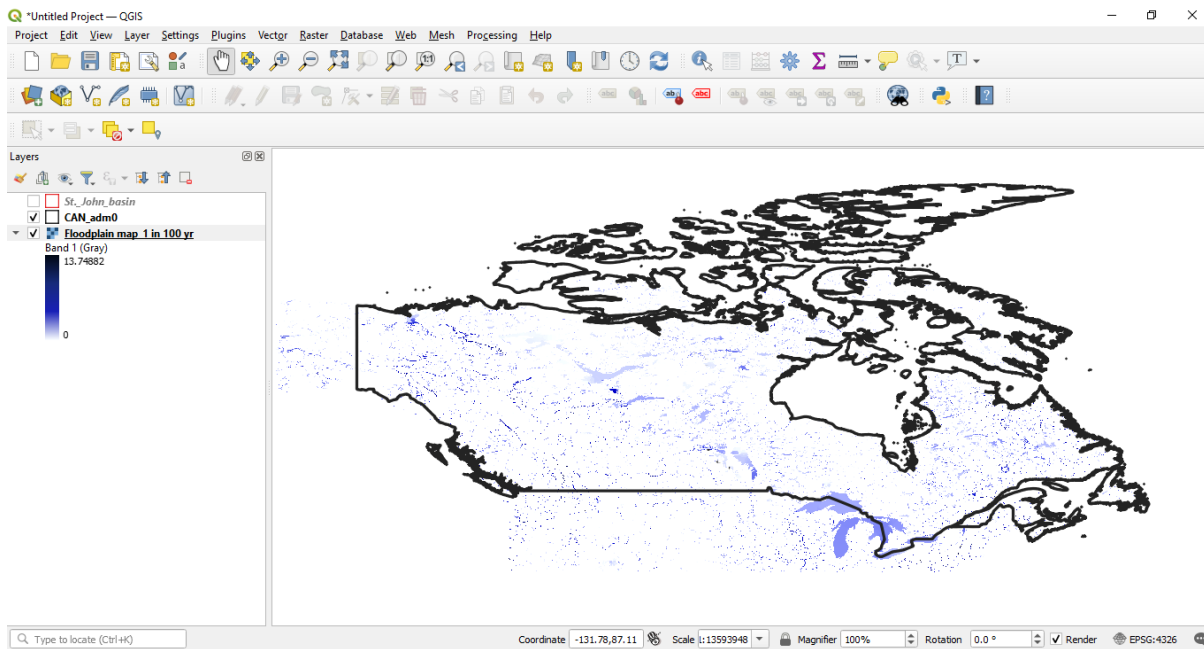


Figure 4.14: A representative 1 in a 100-yr floodplain map of Canada opened in QGIS

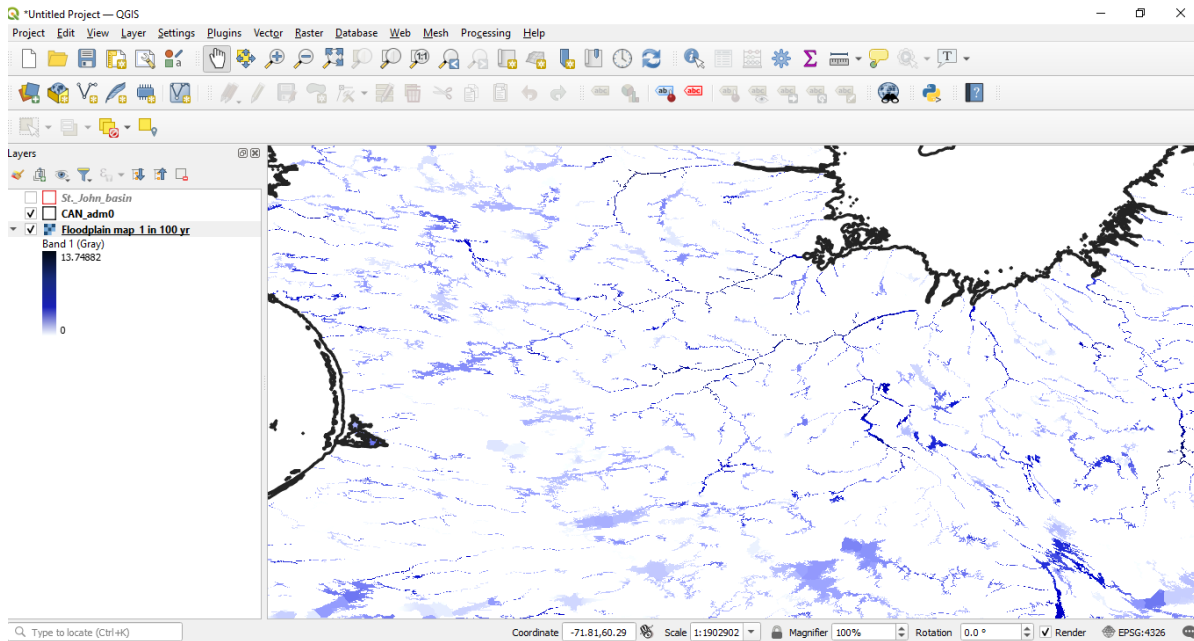


Figure 4.15: Zoomed illustration of 1 in a 100-yr floodplain map opened in QGIS

4.6 Clipping simulated floodplain map for a regional watershed

Once the Canada-wide floodplain map is created, the user can clip a portion of it for regional analysis based on the requirements. It is desirable that the regional study area should contain the same projection as the Canada-wide floodplain map to ensure exact coverage, and overlapping. For a sample example, we have overlaid the St. John basin shapefile (vector format) over the Canada-wide floodplain map (raster format) (**Figure 4.16**). In the next step, the clipping procedure can be implemented. This option can be found by visiting- Raster> Clip by extent (**Figure 4.17**). Upon entering the raster and vector file, the clipping process starts and will, at last, provide the floodplain map for St. John basin (**Figure 4.18**).

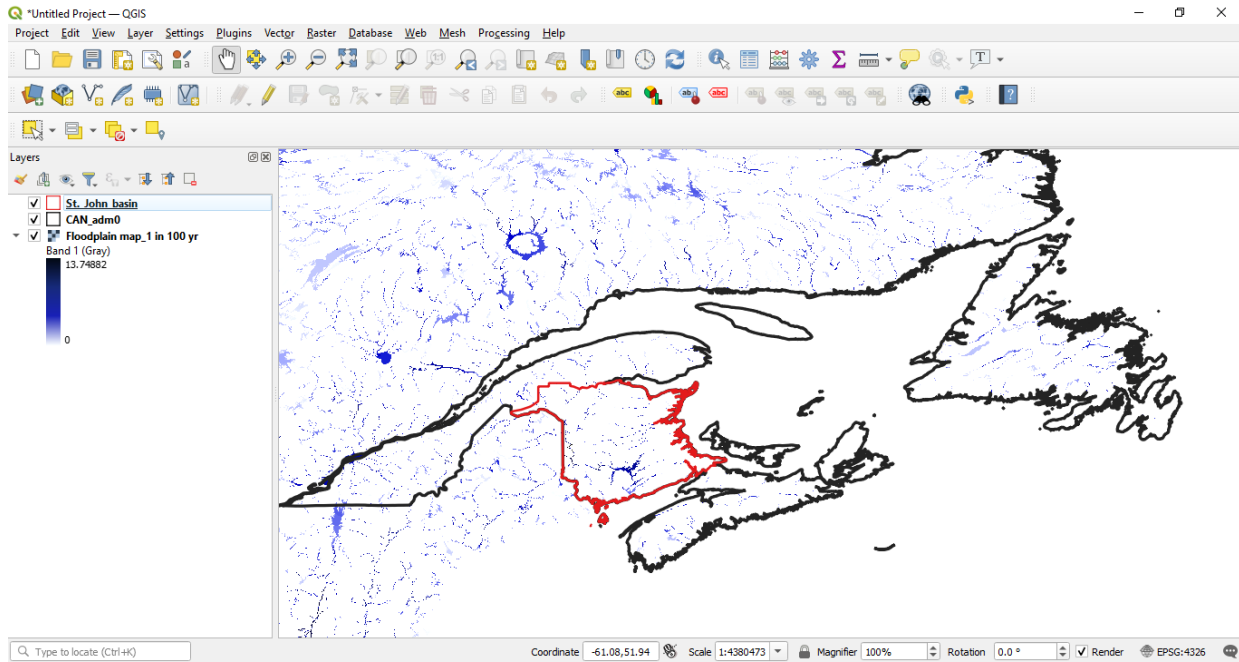


Figure 4.16: Zoomed illustration of 1 in a 100-yr floodplain map opened in QGIS.

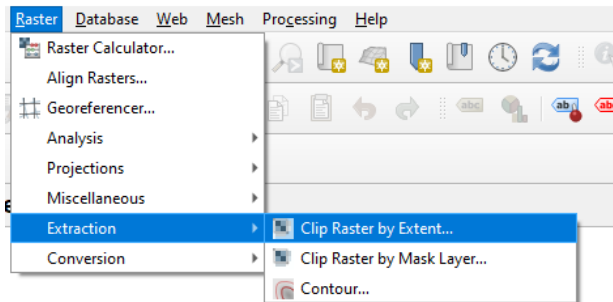


Figure 4.17: Raster clipping in QGIS.

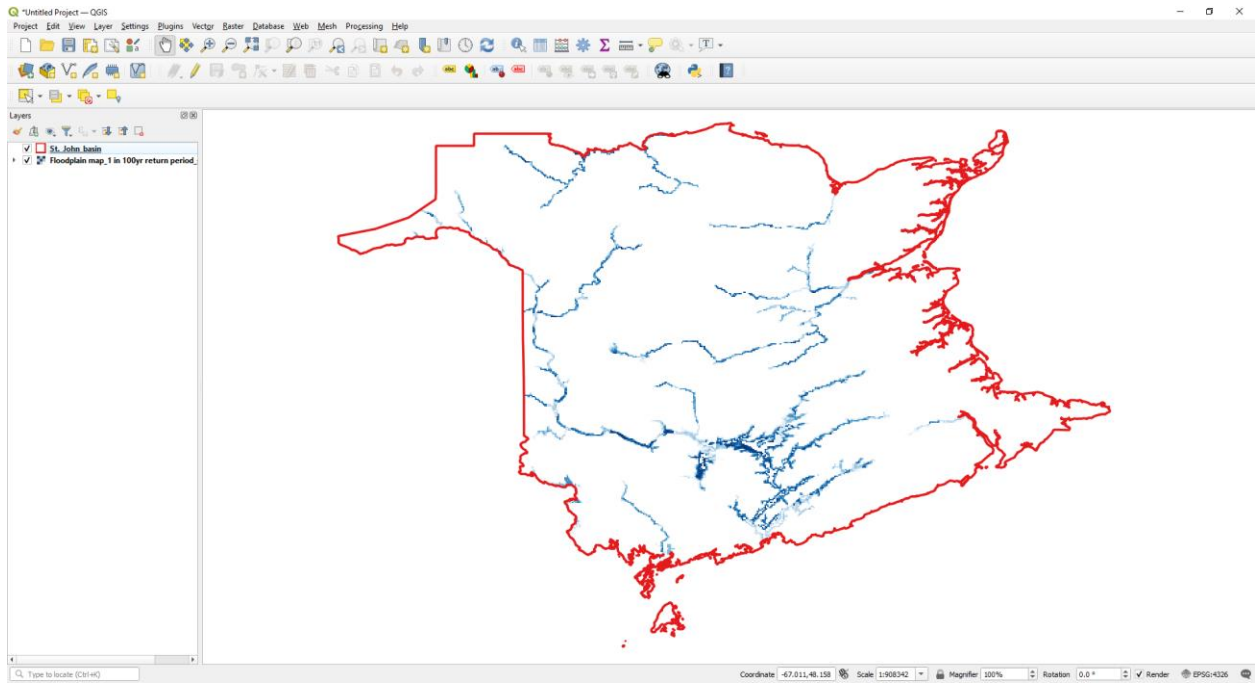


Figure 4.18: Clipped floodplain map of St. John basin from the Canada-wide floodplain map.

5. Closing Remarks

Climate change has contributed significantly to the intensification of several hydro-climatological extremes, including flood disasters. Several regions worldwide are facing increased occurrences of floods, which has amplified the mortality and economic damages year after year. Therefore, identifying the future flooding patterns and their associated impacts has been a major area of research for both the scientific community (e.g. water scientists, hydrologists, and flood modellers) and administrative bodies (e.g. federal government, stakeholders, and policymakers). In the process of understanding climate change impacts, most often, the climate models or GCMs have been used. Rapid developments in climate and atmospheric sciences and other allied areas have improved the efficiency of these models in capturing future scenarios more comprehensively

This report provides a detailed overview of the past and ongoing research on large-scale floodplain mapping with climate change impacts and the availability of public datasets to serve as model inputs. In doing so, we also present a sample simulation of a flood model run with CaMa-Flood model by utilizing runoff input from a CMIP6 GCM. The CaMa-Flood model explicitly parameterizes the sub-grid scale topography of a floodplain, thus describing floodplain inundation dynamics. The relationship between water storage, water level, and flooded area in the model is decided on the basis of the sub-grid scale topographic parameters based on 1 km resolution digital elevation model. In this report, we use R programming language to read, prepare inputs, and analyze most data. The major advantage in using R is that anyone can fix bugs and add features; it also allows integration with other languages like, C/C++, Java, Python, and enables communication with many data sources and other statistical packages. In the last part, we also present a new methodology to convert the output data into a simple GeoTIFF format, which can be used by any non-computational expert. We also describe how one can use the entire floodplain map to clip a portion of the watershed for regional floodplain mapping. This report may be considered by any water professional and expert, working on floodplain mapping to delineate precise floodplain maps and quantify the impacts of climate change.

References

- Alfieri, L., Bisselink, B., Dottori, F., Naumann, G., de Roo, A., Salamon, P., ... & Feyen, L. (2017). Global projections of river flood risk in a warmer world. *Earth's Future*, 5(2), 171-182.
- Arnell, N. W., & Lloyd-Hughes, B. (2014). The global-scale impacts of climate change on water resources and flooding under new climate and socio-economic scenarios. *Climatic change*, 122(1), 127-140.
- Bajracharya, A. R., Bajracharya, S. R., Shrestha, A. B., & Maharjan, S. B. (2018). Climate change impact assessment on the hydrological regime of the Kaligandaki Basin, Nepal. *Science of the Total Environment*, 625, 837-848.
- Bates, P. D., Horritt, M. S., & Fewtrell, T. J. (2010). A simple inertial formulation of the shallow water equations for efficient two-dimensional flood inundation modelling. *Journal of Hydrology*, 387(1-2), 33-45.
- Burn, D. H., & Whitfield, P. H. (2016). Changes in floods and flood regimes in Canada. *Canadian Water Resources Journal/Revue canadienne des ressources hydriques*, 41(1-2), 139-150.
- Bush, Elizabeth J., John W. Loder, Thomas S. James, Linda D. Mortsch, and Stewart J. Cohen. 2014. "An Overview of Canada's Changing Climate." In *Canada in a Changing Climate: Sector Perspectives on Impacts and Adaptation*, edited by F.J. Warren and D.S. Lemmen, 23–64. Ottawa, ON: Government of Canada.
- Clavet-Gaumont, J., Huard, D., Frigon, A., Koenig, K., Slota, P., Rousseau, A., ... & Larouche, B. (2017). Probable maximum flood in a changing climate: An overview for Canadian basins. *Journal of Hydrology: Regional Studies*, 13, 11-25.
- Curry, C. L., Islam, S. U., Zwiers, F. W., & Déry, S. J. (2019). Atmospheric rivers increase future flood risk in Western Canada's largest Pacific river. *Geophysical Research Letters*, 46(3), 1651-1661.
- Dottori, F., Szewczyk, W., Ciscar, J. C., Zhao, F., Alfieri, L., Hirabayashi, Y., ... & Feyen, L. (2018). Increased human and economic losses from river flooding with anthropogenic warming. *Nature Climate Change*, 8(9), 781-786.
- Emori, S., Taylor, K., Hewitson, B., Zermoglio, F., Jukes, M., Lautenschlager, M., & Stockhause, M. (2016). CMIP5 data provided at the IPCC Data Distribution Centre. Fact Sheet of the task group on data and scenario support for impact and climate analysis (TGICA) of the intergovernmental panel on climate change (IPCC), 8.
- Eyring, V., Bony, S., Meehl, G. A., Senior, C. A., Stevens, B., Stouffer, R. J., & Taylor, K. E. (2016). Overview of the Coupled Model Intercomparison Project Phase 6 (CMIP6) experimental design and organization. *Geoscientific Model Development*, 9(5), 1937-1958.
- Farsani, I. F., Farzaneh, M. R., Besalatpour, A. A., Salehi, M. H., & Faramarzi, M. (2019). Assessment of the impact of climate change on spatiotemporal variability of blue and green water resources under CMIP3 and CMIP5 models in a highly mountainous watershed. *Theoretical and Applied Climatology*, 136(1), 169-184.

- Ferrero, B., Tonelli, M., Marcello, F., & Wainer, I. (2021). Long-term Regional Dynamic Sea Level Changes from CMIP6 Projections. *Advances in Atmospheric Sciences*, 38(2), 157-167.
- Gao, C., Liu, L., Ma, D., He, K., & Xu, Y. P. (2019). Assessing responses of hydrological processes to climate change over the southeastern Tibetan Plateau based on resampling of future climate scenarios. *Science of the Total Environment*, 664, 737-752.
- Gaur, A., Gaur, A., & Simonovic, S. P. (2018). Future changes in flood hazards across Canada under a changing climate. *Water*, 10(10), 1441.
- Gaur, A., Gaur, A., Yamazaki, D., & Simonovic, S. P. (2019). Flooding Related Consequences of Climate Change on Canadian Cities and Flow Regulation Infrastructure. *Water*, 11(1), 63.
- Gusain, A., Ghosh, S., & Karmakar, S. (2020). Added value of CMIP6 over CMIP5 models in simulating Indian summer monsoon rainfall. *Atmospheric Research*, 232, 104680.
- Henstra, D., & Thistlethwaite, J. (2017). Climate change, floods, and municipal risk sharing in Canada. Institute on Municipal Finance and Governance.
- Hirabayashi, Y., Mahendran, R., Koirala, S., Konoshima, L., Yamazaki, D., Watanabe, S., ... & Kanae, S. (2013). Global flood risk under climate change. *Nature Climate Change*, 3(9), 816-821.
- Hoch, J. M., & Trigg, M. A. (2019). Advancing global flood hazard simulations by improving comparability, benchmarking, and integration of global flood models. *Environmental Research Letters*, 14(3), 034001.
- IPCC (2007) Contribution of Working Group I to the Fourth Assessment Report of the Intergovernmental Panel on Climate Change. Solomon S, Qin D, Manning M, Chen Z, Marquis M, Averyt KB, Tignor M, Miller HL (eds). Cambridge University Press, Cambridge, United Kingdom and New York, NY, USA
- Jongman, B., Ward, P. J., & Aerts, J. C. (2012). Global exposure to river and coastal flooding: Long term trends and changes. *Global Environmental Change*, 22(4), 823-835.
- Knutti, R., Masson, D., & Gettelman, A. (2013). Climate model genealogy: Generation CMIP5 and how we got there. *Geophysical Research Letters*, 40(6), 1194-1199.
- Kushnir, Y., Scaife, A. A., Arritt, R., Balsamo, G., Boer, G., Doblas-Reyes, F., ... & Wu, B. (2019). Towards operational predictions of the near-term climate. *Nature Climate Change*, 9(2), 94-101.
- Lawrence, D. M., Hurtt, G. C., Arneth, A., Brovkin, V., Calvin, K. V., Jones, A. D., ... & Shevliakova, E. (2016). The Land Use Model Intercomparison Project (LUMIP) contribution to CMIP6: rationale and experimental design. *Geoscientific Model Development*, 9(9), 2973-2998.
- Masutomi, Y., Inui, Y., Takahashi, K., & Matsuoka, Y. (2007). Global Drainage Basin Database (GDBD).
- Meehl, G. A. (1995). Global coupled general circulation models. *Bulletin of the American Meteorological Society*, 76(6), 951-957.

- Meehl, G. A., Boer, G. J., Covey, C., Latif, M., & Stouffer, R. J. (2000). The coupled model intercomparison project (CMIP). *Bulletin of the American Meteorological Society*, 81(2), 313-318.
- Meehl, G. A., Covey, C., Delworth, T., Latif, M., McAvaney, B., Mitchell, J. F., ... & Taylor, K. E. (2007). The WCRP CMIP3 multimodel dataset: A new era in climate change research. *Bulletin of the American meteorological society*, 88(9), 1383-1394.
- Meehl, G. A., Moss, R., Taylor, K. E., Eyring, V., Stouffer, R. J., Bony, S., & Stevens, B. (2014). Climate model intercomparisons: Preparing for the next phase. *Eos, Transactions American Geophysical Union*, 95(9), 77-78.
- Milly, P. C. D., Wetherald, R. T., Dunne, K. A., & Delworth, T. L. (2002). Increasing risk of great floods in a changing climate. *Nature*, 415(6871), 514-517.
- Mohanty, M. P., & Simonovic, S. P. (2021). Understanding dynamics of population flood exposure in Canada with multiple high-resolution population datasets. *Science of The Total Environment*, 759, 143559.
- Oubennaceur, K., Chokmani, K., Nastev, M., Lhissou, R., & El Alem, A. (2019). Flood risk mapping for direct damage to residential buildings in Quebec, Canada. *International journal of disaster risk reduction*, 33, 44-54.
- Pappenberger, F., Dutra, E., Wetterhall, F., & Cloke, H. L. (2012). Deriving global flood hazard maps of fluvial floods through a physical model cascade. *Hydrology and Earth System Sciences*, 16(11), 4143-4156.
- Public Safety Canada (2019) Public Safety Canada (2019) < <https://www.publicsafety.gc.ca/cnt/mrgnc-mngmnt/dsstr-prvntn-mtght/ndmp/fldpln-mppng-en.aspx>> accessed on 10 May 2020
- Rentschler, J., & Salhab, M. (2020). People in Harm's Way: Flood Exposure and Poverty in 189 Countries <https://elibrary.worldbank.org/doi/abs/10.1596/1813-9450-9447> accessed on 22 June 2021..
- Samiran, D., & Simonovic, S. P. (2012). Assessment of uncertainty in flood flows under climate change impacts in the Upper Thames River basin, Canada. *British Journal of Environment and Climate Change*, 2(4), 318-338.
- Taylor, K. E., Stouffer, R. J., & Meehl, G. A. (2012). An overview of CMIP5 and the experiment design. *Bulletin of the American meteorological Society*, 93(4), 485-498.
- Taylor, K.E., Stouffer, R.J., & Meehl, G.A. (2011) A Summary of the CMIP5 Experiment Design < https://web.archive.org/web/20170120012654/http://cmip.llnl.gov/cmip5/docs/Taylor_CMIP_5_design.pdf> accessed on 4 March 2021.
- Touzé-Peiffer, L., Barberousse, A., & Le Treut, H. (2020). The Coupled Model Intercomparison Project: History, uses, and structural effects on climate research. *Wiley Interdisciplinary Reviews: Climate Change*, 11(4), e648.

- Trenberth, K. E., & Asrar, G. R. (2012). Challenges and opportunities in water cycle research: WCRP contributions. *The Earth's Hydrological Cycle*, 515-532.
- Trigg, M. A., Birch, C. E., Neal, J. C., Bates, P. D., Smith, A., Sampson, C. C., ... & Ward, P. J. (2016). The credibility challenge for global fluvial flood risk analysis. *Environmental Research Letters*, 11(9), 094014.
- Webb, M. J., Andrews, T., Bodas-Salcedo, A., Bony, S., Bretherton, C. S., Chadwick, R., ... & Watanabe, M. (2017). The cloud feedback model intercomparison project (CFMIP) contribution to CMIP6. *Geoscientific Model Development*, 10(1), 359-384.
- Wing, O. E., Bates, P. D., Smith, A. M., Sampson, C. C., Johnson, K. A., Fargione, J., & Morefield, P. (2018). Estimates of present and future flood risk in the conterminous United States. *Environmental Research Letters*, 13(3), 034023.
- Winsemius, H. C., Aerts, J. C., Van Beek, L. P., Bierkens, M. F., Bouwman, A., Jongman, B., ... & Ward, P. J. (2016). Global drivers of future river flood risk. *Nature Climate Change*, 6(4), 381-385.
- Yamazaki, D., de Almeida, G. A., & Bates, P. D. (2013). Improving computational efficiency in global river models by implementing the local inertial flow equation and a vector-based river network map. *Water Resources Research*, 49(11), 7221-7235.
- Yamazaki, D., Kanae, S., Kim, H., & Oki, T. (2011). A physically based description of floodplain inundation dynamics in a global river routing model. *Water Resources Research*, 47(4).
- Yamazaki, D., Oki, T., & Kanae, S. (2009). Deriving a global river network map and its sub-grid topographic characteristics from a fine-resolution flow direction map. *Hydrology and Earth System Sciences*, 13(11), 2241.
- Yamazaki, D., O'Loughlin, F., Trigg, M. A., Miller, Z. F., Pavelsky, T. M., & Bates, P. D. (2014). Development of the global width database for large rivers. *Water Resources Research*, 50(4), 3467-3480.
- Yamazaki, D., Trigg, M. A., & Ikeshima, D. (2015). Development of a global~ 90 m water body map using multi-temporal Landsat images. *Remote Sensing of Environment*, 171, 337-351. Yamazaki, D., Ikeshima, D., Sosa, J., Bates, P. D., Allen, G. H., & Pavelsky, T. M. (2019). MERIT Hydro: a high-resolution global hydrography map based on latest topography dataset. *Water Resources Research*, 55(6), 5053-5073.

Appendix A: Previous Reports in the Series

Samiran Das and Slobodan P. Simonovic (2012). Assessment of Uncertainty in Flood Flows under Climate Change. Water Resources Research Report no. 079, Facility for Intelligent Decision Support, Department of Civil and Environmental Engineering, London, Ontario, Canada, 67 pages. ISBN: (print) 978-0-7714-2960-6; (online) 978-0-7714-2961-3. Rubaiya

Sarwar, Sarah E. Irwin, Leanna King and Slobodan P. Simonovic (2012). Assessment of Climatic Vulnerability in the Upper Thames River basin: Downscaling with SDSM. Water Resources Research Report no. 080, Facility for Intelligent Decision Support, Department of Civil and Environmental Engineering, London, Ontario, Canada, 65 pages. ISBN: (print) 978-0-7714-2962-0; (online) 978-0-7714-2963-7.

Sarah E. Irwin, Rubaiya Sarwar, Leanna King and Slobodan P. Simonovic (2012). Assessment of Climatic Vulnerability in the Upper Thames River basin: Downscaling with LARS-WG. Water Resources Research Report no. 081, Facility for Intelligent Decision Support, Department of Civil and Environmental Engineering, London, Ontario, Canada, 80 pages. ISBN: (print) 978-0-7714-2964-4; (online) 978-0-7714-2965-1.

Samiran Das and Slobodan P. Simonovic (2012). Guidelines for Flood Frequency Estimation under Climate Change. Water Resources Research Report no. 082, Facility for Intelligent Decision Support, Department of Civil and Environmental Engineering, London, Ontario, Canada, 44 pages. ISBN: (print) 978-0-7714-2973-6; (online) 978-0-7714-2974-3.

Angela Peck and Slobodan P. Simonovic (2013). Coastal Cities at Risk (CCaR): Generic System Dynamics Simulation Models for Use with City Resilience Simulator. Water Resources Research Report no. 083, Facility for Intelligent Decision Support, Department of Civil and Environmental Engineering, London, Ontario, Canada, 55 pages. ISBN: (print) 978-0-7714-3024-4; (online) 978-0-7714-3025-1.

Roshan Srivastav and Slobodan P. Simonovic (2014). Generic Framework for Computation of Spatial Dynamic Resilience. Water Resources Research Report no. 085, Facility for Intelligent Decision Support, Department of Civil and Environmental Engineering, London, Ontario, Canada, 81 pages. ISBN: (print) 978-0-7714-3067-1; (online) 978-0-7714-3068-8.

Angela Peck and Slobodan P. Simonovic (2014). Coupling System Dynamics with Geographic Information Systems: CCaR Project Report. Water Resources Research Report no. 086, Facility 56 for Intelligent Decision Support, Department of Civil and Environmental Engineering, London, Ontario, Canada, 60 pages. ISBN: (print) 978-0-7714-3069-5; (online) 978-0-7714-3070-1.

Sarah Irwin, Roshan Srivastav and Slobodan P. Simonovic (2014). Instruction for Watershed Delineation in an ArcGIS Environment for Regionalization Studies. Water Resources Research Report no. 087, Facility for Intelligent Decision Support, Department of Civil and Environmental Engineering, London, Ontario, Canada, 45 pages. ISBN: (print) 978-0-7714-3071-8; (online) 978-0-7714-3072-5.

Andre Schardong, Roshan K. Srivastav and Slobodan P. Simonovic (2014). Computerized Tool for the Development of Intensity-Duration-Frequency Curves under a Changing Climate: Users Manual v.1. Water Resources Research Report no. 088, Facility for Intelligent Decision Support, Department of Civil and Environmental Engineering, London, Ontario, Canada, 68 pages. ISBN: (print) 978-0-7714-3085-5; (online) 978-0-7714-3086-2.

Roshan K. Srivastav, Andre Schardong and Slobodan P. Simonovic (2014). Computerized Tool for the Development of Intensity-Duration-Frequency Curves under a Changing Climate: Technical Manual v.1. Water Resources Research Report no. 089, Facility for Intelligent Decision Support, Department of Civil

and Environmental Engineering, London, Ontario, Canada, 62 pages. ISBN: (print) 978-0-7714-3087-9; (online) 978-0-7714-3088-6.

Roshan K. Srivastav and Slobodan P. Simonovic (2014). Simulation of Dynamic Resilience: A Railway Case Study. Water Resources Research Report no. 090, Facility for Intelligent Decision Support, Department of Civil and Environmental Engineering, London, Ontario, Canada, 91 pages. ISBN: (print) 978-0-7714-3089-3; (online) 978-0-7714-3090-9.

Nick Agam and Slobodan P. Simonovic (2015). Development of Inundation Maps for the Vancouver Coastline Incorporating the Effects of Sea Level Rise and Extreme Events. Water Resources Research Report no. 091, Facility for Intelligent Decision Support, Department of Civil and Environmental Engineering, London, Ontario, Canada, 107 pages. ISBN: (print) 978-0-7714-3092-3; (online) 978-0-7714-3094-7.

Sarah Irwin, Roshan K. Srivastav and Slobodan P. Simonovic (2015). Instructions for Operating the Proposed Regionalization Tool "Cluster-FCM" Using Fuzzy C-Means Clustering and LMoment Statistics. Water Resources Research Report no. 092, Facility for Intelligent Decision Support, Department of Civil and Environmental Engineering, London, Ontario, Canada, 54 pages. ISBN: (print) 978-0-7714-3101-2; (online) 978-0-7714-3102-9. 57

Bogdan Pavlovic and Slobodan P. Simonovic (2016). Automated Control Flow Generation Procedure: Cheakamus Dam Case Study. Water Resources Research Report no. 093, Facility for Intelligent Decision Support, Department of Civil and Environmental Engineering, London, Ontario, Canada, 78 pages. ISBN: (print) 978-0-7714-3113-5; (online) 978-0-7714-3114-2.

Sarah Irwin, Slobodan P. Simonovic and Niru Nirupama (2016). Introduction to ResilSIM: A Decision Support Tool for Estimating Disaster Resilience to Hydro-Meteorological Events. Water Resources Research Report no. 094, Facility for Intelligent Decision Support, Department of Civil and Environmental Engineering, London, Ontario, Canada, 66 pages. ISBN: (print) 978-0-7714-3115-9; (online) 978-0-7714-3116-6.

Tommy Kokas, Slobodan P. Simonovic (2016). Flood Risk Management in Canadian Urban Environments: A Comprehensive Framework for Water Resources Modeling and Decision- Making. Water Resources Research Report no. 095. Facility for Intelligent Decision Support, Department of Civil and Environmental Engineering, London, Ontario, Canada, 66 pages. ISBN: (print) 978-0-7714-3117-3; (online) 978-0-7714-3118-0.

Jingjing Kong and Slobodan P. Simonovic (2016). Interdependent Infrastructure Network Resilience Model with Joint Restoration Strategy. Water Resources Research Report no. 096, Facility for Intelligent Decision Support, Department of Civil and Environmental Engineering, London, Ontario, Canada, 83 pages. ISBN: (print) 978-0-7714-3132-6; (online) 978-0-7714-3133-3.

Sohom Mandal, Patrick A. Breach and Slobodan P. Simonovic (2017). Tools for Downscaling Climate Variables: A Technical Manual. Water Resources Research Report no. 097, Facility for Intelligent Decision Support, Department of Civil and Environmental Engineering, London, Ontario, Canada, 95 pages. ISBN: (print) 978-0-7714-3135-7; (online) 978-0-7714-3136-4.

R Arunkumar and Slobodan P. Simonovic (2017). General Methodology for Developing a CFD Model for Studying Spillway Hydraulics using ANSYS Fluent. Water Resources Research Report no. 098, Facility for Intelligent Decision Support, Department of Civil and Environmental Engineering, London, Ontario, Canada, 39 pages. ISBN: (print) 978-0-7714-3148-7; (online) 978-0-7714-3149-4.

Andre Schardong, Slobodan P. Simonovic and Dan Sandink (2017). Computerized Tool for the Development of Intensity-Duration-Frequency Curves Under a Changing Climate: Technical Manual v.2.1.

Water Resources Research Report no. 099, Facility for Intelligent Decision Support, Department of Civil and Environmental Engineering, London, Ontario, Canada, 52 pages. ISBN: (print) 978-0-7714-3150-0; (online) 978-0-7714-3151-7. 58

Andre Schardong, Slobodan P. Simonovic and Dan Sandink (2017). Computerized Tool for the Development of Intensity-Duration-Frequency Curves Under a Changing Climate: User's Manual v.2.1. Water Resources Research Report no. 100, Facility for Intelligent Decision Support, Department of Civil and Environmental Engineering, London, Ontario, Canada, 52 pages. ISBN: (print) 978-0-7714-3152-4; (online) 978-0-7714-3153-1.

Ayushi Gaur, Abhishek Gaur and Slobodan P. Simonovic (2017). Modelling of High Resolution Flow from GCM Simulated Runoff using a Mesoscale Hydrodynamic Model: CAMA-FLOOD. Water Resources Research Report no. 101, Facility for Intelligent Decision Support, Department of Civil and Environmental Engineering, London, Ontario, Canada, 44 pages. ISBN: (print) 978-0-7714-3154-8; (online) 978-0-7714-3155-5.

Jingjing Kong and Slobodan P. Simonovic (2017). Multi-hazard resilience model of an interdependent infrastructure system. Water Resources Research Report no. 102, Facility for Intelligent Decision Support. Department of Civil and Environmental Engineering, London, Ontario, Canada, 99 pages. ISBN: (print) 978-0-7714-3158-6; (online) 978-0-7714-3159-3.

Andre Schardong, Slobodan P. Simonovic and Dan Sandink (2018). Computerized Tool for the Development of Intensity-Duration-Frequency Curves Under a Changing Climate: Technical Manual v.3. Water Resources Research Report no. 103, Facility for Intelligent Decision Support, Department of Civil and Environmental Engineering, London, Ontario, Canada, 67 pages. ISBN: 978-0-7714-3107-4.

Andre Schardong, Slobodan P. Simonovic and Dan Sandink (2018). Computerized Tool for the Development of Intensity-Duration-Frequency Curves Under a Changing Climate: User's Manual v.3. Water Resources Research Report no. 104, Facility for Intelligent Decision Support, Department of Civil and Environmental Engineering, London, Ontario, Canada, 80 pages. ISBN: 978-0-7714-3108-1.

Schardong, A., S. P. Simonovic and H. Tong (2018). Use of Quantitative Resilience in Managing Urban Infrastructure Response to Natural Hazards: A Web-Based Decision Support Tool - ResilSIMt. Water Resources Research Report no. 105, Facility for Intelligent Decision Support, Department of Civil and Environmental Engineering, London, Ontario, Canada, 112 pages. ISBN: 978-0-7714-3115-7.

Feitoza Silva D. and S. P. Simonovic (2020). Development of Non-Stationary Rainfall Intensity Duration Frequency Curves for Future Climate Conditions. Water Resources Research Report no. 106, Facility for Intelligent Decision Support, Department of Civil and Environmental Engineering, London, Ontario, Canada, 48 pages. ISBN: (print) 978-0-7714-3137-1; (online) 978-0-7714-3138-8.

Braden, J. and S.P. Simonovic (2020). A Review of Flood Hazard Mapping Practices across Canada. Water Resources Research Report no. 107, Facility for Intelligent Decision Support, Department of Civil and Environmental Engineering, London, Ontario, Canada, 64 pages. ISBN: (print) 978-0-7714-3143-2; (online) 978-0-7714-3144-9.

Patrick A. Breach and Slobodan P. Simonovic (2020). ANEMI 3: Tool for investigating impacts of global change. Water Resources Research Report no. 108, Facility for Intelligent Decision Support, Department of Civil and Environmental Engineering, London, Ontario, Canada, 134 pages. ISBN: (print) 978-0-7714-3145-6; (online) 978-0-7714-3146-3.

Mohit P. Mohanty and Slobodan P. Simonovic (2020). A comprehensive framework for regional floodplain mapping. Water Resources Research Report no. 109, Facility for Intelligent Decision Support, Department

of Civil and Environmental Engineering, London, Ontario, Canada, 58 pages. ISBN: (print) 978-0-7714-3147-0 ; (online) 978-0-7714-3148-7.

Bogdana Sredojevic, Mohit P. Mohanty and Slobodan P. Simonovic (2020). Regional Analysis of Population Exposure to Flooding in Canada. Water Resources Research Report no. 110, Facility for Intelligent Decision Support, Department of Civil and Environmental Engineering, London, Ontario, Canada, 61 pages. ISBN: (print) 978-0-7714-3151-7; (online) 978-0-7714-3152-4.

Haiyan Jiang, and Slobodan P. Simonovic (2021) ANEMI_Yangtze A regional integrated assessment model for the Yangtze Economic Belt in China. Water Resources Research Report no. 111, Facility for Intelligent Decision Support, Department of Civil and Environmental Engineering, London, Ontario, Canada, 61 pages. ISBN: (print) 978-0-7714-3155-5; (online) 978-0-7714-3156-2.